ISSN 0280–5316
ISRN LUTFD2/TFRT--5556--SE

Multivariable System Identification of Human Postural Control

A Subspace Method Approach

Jonas Ekblad

Department of Automatic Control
Lund Institute of Technology
March 1996

Multivariable System Identification of Human Postural Control

A Subspace Method Approach

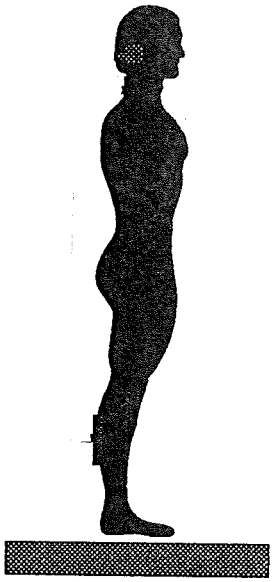

by
Jonas Ekblad

Supervisors: Rolf Johansson and Måns Magnusson

Department of Automatic Control, Lund Institute of Technology
March 1995

Department of Automatic Control
Lund Institute of Technology
P.O. Box 118
S-221 00 Lund Sweden

Document name
MASTER THESIS

Date of issue
March 1996

Document Number
ISRN LUTFD2/TFRT--5556--SE

Author(s)
Jonas Ekblad

Supervisors
Rolf Johansson and Måns Magnusson

Sponsoring organisation

Title and subtitle
Multivariable Identification of Human Postural Control – A Subspace Method Approach.

Abstract

In order to analyse the human postural control system single-stimulus multi-response measurement experiments are made, where the body sway due to an induced disturbance on the calf muscles are recorded with force platforms, Selspot systems or EMG-equipments. The measured outputs are usually analysed one by one as for a Single-Input Single-Output system. In this study a Single-Input Multi-Output approach, consisting of a subspace state-space algorithm, is used to map the stimulus-response relation.

A generated Pseudo-Random-Binary-Sequence signal was used to induce sway to the test subject. A six axis contact force-state was measured by a force platform and the position of the body mass centre was recorded with a Diode-CCD-camera system. Tests were made on seven normal subjects with large and small amplitude calf stimulation and the subjects were tested both with closed and open eyes.

Of the nine recorded outputs (three contact forces, three torques and three space coordinates) three were found to be relevant in the identification of calf muscle stimulation. These were the sagittal shear force, the torque around the lateral axis and the sagittal position coordinate of the body mass centre. A linear dependence between shear force and torque was found, and there was a strong correlation between all the three outputs. The subspace algorithm can acceptably identify the postural control system of closed eyes, but not the system of open eyes.

The subspace method is able to analyse disturbed systems, but lacks of correct noise model. The white noise assumption made in the algorithm is not justified. This leads to difficulties in locating a correct model order, balanced model reduction approximation or statistical residual tests together with system simulation can be used as a method of model validation.

Key words

Classification system and/or index terms (if any)

Supplementary bibliographical information

ISSN and key title
0280–5316

ISBN

Language
English

Number of pages
48

Recipient's notes

Security classification

Contents

1 Introduction

Several human control systems show a multiple output behaviour even though only one input (disturbance) is induced on the body. Identification of multivariable systems, so called multiple-input multiple-output (MIMO) systems, is therefore a important field of the analysis of human systems. An often used approach to MIMO identification is the ARMAX-models. Multivariable systems however generally (unlike single variable systems) lack an unique factorisation of the transfer function ($H(z^{-1})$) into the input and output polynomials ($A(z^{-1})$ and $B(z^{-1})$) [Johansson 93]. A major drawback with ARMAX-identification is therefore the difficulty with model class selection and overparametrization of the model.
The state space methods are another class of methods for MIMO identification. All these methods has the state-space representation of the system as starting point for the identification. In state-space representation there are no principal differences between the SISO (Single-Input Single-Output) case and the MIMO case, which is a great advantage especially when exploiting a system. One class of the state-space methods is the subspace model algorithms ([Moonen et al 89], [Verhaegen and Dewilde 92] and [Johansson 95]), where just a finite set of input-output data points, without any prior identification, is required to determine the system matrices. The main characteristic of the algorithms is the computation, by means of two singular value decomposition, of a subspace defined from input-output data organised in Hankel matrices.
In this paper the algorithms proposed by [Moonen et al 89] and [Johansson 95] were used to identify the system matrices of human postural control. In §2 the mathematical description of the algorithms are presented combined with a brief physiological background of human postural control, the section ends with a presentation of simulations done with the algorithms. In section 3 the materials and methods are described, the results of the two pilot tests and the main study are presented in §4 together with an approach of stochastic realisation of the residuals. The report ends with a discussion of the results and conclusions that can be drawn from the study.

2 Mathematical and physiological background

2.1 A brief physiological background

The system of human postural control consists of several partly independent sensory receptor systems. These are vision, the vestibular organ in the inner ear, pressor sensors, proprioceptive sensors and anticipation [Johansson and Magnusson 91]. When the calf muscles are disturbed by stimulation the postural control system are exposed to erroneous proprioceptive information [Pyykkö et al 83], the proprioceptive inputs play an important role in the regulation of posture [Dietz 92]. When a person is exposed to a sagittal disturbance, the equilibrium might according to Nashner be regain by two control strategies [Johansson and Magnusson 91]: "ankle strategy", where the body is rotated around the ankles like an one-segmented inverted pendulum, or "hip strategy" where the hips and/or knees are flexed. The person's movement might be a combination of these two. The ankle strategy is employed to counter small disturbances and involves mainly torques at the person's feet and the ground (force platform). The hip strategy is used when large disturbances (the person is close to falling) have to be overcome, here the shear forces against the supporting surface play an important role to maintain the equilibrium [Johansson et al 88].

2.2 Theory of subspace state-space methods

The main idea behind subspace identification is the singular value decomposition of matrices containing input-output data and the partition of the state matrix into two time shifted state matrices, which together span a subspace of the same length as n, the minimal system order. The following algorithm can be found in [Moonen et al 89] and in [Johansson 95].
Starting point is the discrete, time-invariant and linear state-space representation with m inputs and p outputs

$$x_{k+1} = Ax_k + Bu_k + w_k$$
$$y_k = Cx_k + Du_k + e_k$$

with the input u_k ($\in \Re^m$), output y_k ($\in \Re^p$), state vector x_k ($\in \Re^n$) and the noise sequences w_k ($\in \Re^n$) and e_k ($\in \Re^p$). A, B, C and D are the to be identified system matrices and n denotes the minimal system order. The finite input sequence, with N measurement points, $\{u_k\}_{k=1}^N$ and the corresponding output sequence $\{y_k\}_{k=1}^N$ are then organised into the Hankel matrices.

$$U_h = \begin{pmatrix} u_k & u_{k+1} & \cdot & u_{k+s-1} \\ u_{k+1} & u_{k+2} & \cdot & u_{k+s} \\ \cdot & \cdot & \cdot & \cdot \\ u_{k+r-1} & u_{k+r} & \cdot & u_{k+s+r-2} \end{pmatrix}, \qquad Y_h = \begin{pmatrix} y_k & y_{k+1} & \cdot & y_{k+s-1} \\ y_{k+1} & y_{k+2} & \cdot & y_{k+s} \\ \cdot & \cdot & \cdot & \cdot \\ y_{k+r-1} & y_{k+r} & \cdot & y_{k+s+r-2} \end{pmatrix}$$

Where N>s+r-2 and s corresponds to number of datapoints used in the algorithm and r is the number of block rows. Since s is the number of data points in the Input-Output Hankel matrices, s must be large to insure that enough information of the system is available, i.e., the Hankel matrices must have a very rectangular structure with s>>r.
By repeated substitution in the state-space equation, we receive for just two step:

$$\begin{aligned} y_k &= Cx_k + Du_k, \\ y_{k+1} &= Cx_{k+1} + Du_{k+1} = CAx_k + CBu_k + Du_{k+1}, \\ y_{k+2} &= Cx_{k+2} + Du_{k+2} = CAx_{k+1} + CBu_{k+1} + Du_{k+2}, \end{aligned}$$

which in matrix form equals

$$\begin{pmatrix} y_k & y_{k+1} \\ y_{k+1} & y_{k+2} \end{pmatrix} = \begin{pmatrix} C \\ CA \end{pmatrix} \begin{pmatrix} x_k & x_{k+1} \end{pmatrix} + \begin{pmatrix} D & 0 \\ CB & D \end{pmatrix} \begin{pmatrix} u_k & u_{k+1} \\ u_{k+1} & u_{k+2} \end{pmatrix}$$

If the substitution is concluded, then the following representation describes the input-output relation:

$$Y_h = C_r \cdot X + D_r \cdot U_h$$

where X is a matrix containing the consecutive state vectors

$$X = \begin{pmatrix} x_k & x_{k+1} & x_{k+2} & \cdots & x_{k+s-1} \end{pmatrix}$$

and

$$C_r = \begin{pmatrix} C \\ CA \\ \cdot \\ CA^{r-1} \end{pmatrix}, \qquad D_r = \begin{pmatrix} D & 0 & \cdot & 0 \\ CB & D & \cdot & 0 \\ \cdot & \cdot & \cdot & 0 \\ CA^{r-2}B & CA^{r-3}B & \cdot & D \end{pmatrix}$$

C_r is an extended observability matrix and D_r is a lower triangular Toeplitz matrix, containing the Markov parameters, D, CB, CAB and so forth.
To determine the sequence of state vectors, X is divided into two state vectors with a relative timeshift of j.

$$\begin{aligned} X_1 &= \begin{pmatrix} x_k & x_{k+1} & \cdots & x_{k+s-1} \end{pmatrix} \\ X_2 &= \begin{pmatrix} x_{k+j} & x_{k+j+1} & \cdots & x_{k+j+s-1} \end{pmatrix} \end{aligned}$$

Y_h and U_h are in the same way divided into Y_{h1}, Y_{h2}, U_{h1} and U_{h2},

$$U_{h1} = \begin{pmatrix} u_k & u_{k+1} & \cdot & u_{k+s-1} \\ u_{k+1} & u_{k+2} & \cdot & u_{k+s} \\ \cdot & \cdot & \cdot & \cdot \\ u_{k+r-1} & u_{k+r} & \cdot & u_{k+s+r-2} \end{pmatrix}, \qquad Y_{h1} = \begin{pmatrix} y_k & y_{k+1} & \cdot & y_{k+s-1} \\ y_{k+1} & y_{k+2} & \cdot & y_{k+s} \\ \cdot & \cdot & \cdot & \cdot \\ y_{k+r-1} & y_{k+r} & \cdot & y_{k+s+r-2} \end{pmatrix}$$

$$U_{h2}=\begin{pmatrix} u_{k+j} & u_{k+j+1} & \cdot & u_{k+s+j-1} \\ u_{k+j+1} & u_{k+j+2} & \cdot & u_{k+s+j} \\ \cdot & \cdot & \cdot & \cdot \\ u_{k+r+j-1} & u_{k+r+j} & \cdot & u_{k+s+r+j-2} \end{pmatrix},\ Y_{h2}=\begin{pmatrix} y_{k+j} & y_{k+j+1} & \cdot & y_{k+s+j-1} \\ y_{k+j+1} & y_{k+j+2} & \cdot & y_{k+s+j} \\ \cdot & \cdot & \cdot & \cdot \\ y_{k+r+j-1} & y_{k+r+j} & \cdot & y_{k+s+r+j-2} \end{pmatrix}$$

and then the input-output relation becomes

$$Y_{h1}=C_r\cdot X_1+D_r\cdot U_{h1}$$

$$Y_{h2}=C_r\cdot X_2+D_r\cdot U_{h2}$$

If r>n-1 the two state vectors, X_1 and X_2 can be determined as follows (C_r^+ denotes the pseudo inverse of C_r).

$$X_1=C_r^+(Y_{h1}-D_rU_{h1})=(C_r^+-C_r^+D_r)\begin{pmatrix}Y_{h1}\\U_{h1}\end{pmatrix}$$

$$X_2=C_r^+(Y_{h2}-D_rU_{h2})=(C_r^+-C_r^+D_r)\begin{pmatrix}Y_{h2}\\U_{h2}\end{pmatrix}$$

Since X_2 is a timeshift j before X_1, the two state matrices are related, which easily can be shown by repeated substitution in the state space equation, via

$$X_2=A^jX_1+\begin{pmatrix}A^{j-1}B & \ldots & AB & B\end{pmatrix}U_{h1}=A^jX_1+\mathrm{B}_jU_{h1}$$

$$=A^j(C_r^+-C_r^+D_r)\begin{pmatrix}Y_{h1}\\U_{h1}\end{pmatrix}+\begin{pmatrix}0 & \mathrm{B}_j\end{pmatrix}\begin{pmatrix}Y_{h1}\\U_{h1}\end{pmatrix}$$

X_2 can therefore be determined by linearly combinations of the input-output Hankel matrix

$$Z_1=\begin{pmatrix}Y_{h1}\\U_{h1}\end{pmatrix}$$

Now form in the same way the Hankel matrix Z_2, and let Z be

$$Z=\begin{pmatrix}Z_1\\Z_2\end{pmatrix}$$

The singular value decomposition of Z is

$$Z=U\Sigma V^T=\begin{pmatrix}U_1 & U_1^\perp\end{pmatrix}\begin{pmatrix}\Sigma_{11} & 0\\0 & 0\end{pmatrix}V^T$$

where U and V are unitary matrices ($U^TU=I$) and Σ is a diagonal matrix. The matrix U can be divided into two orthogonal matrices, U_1 and $U_1^\perp$ with $U_1^TU_1^\perp=0$, according to

$$\begin{pmatrix}U_1 & U_1^\perp\end{pmatrix}^T\begin{pmatrix}U_1 & U_1^\perp\end{pmatrix}=\begin{pmatrix}U_1^T\\U_1^{\perp T}\end{pmatrix}\begin{pmatrix}U_1 & U_1^\perp\end{pmatrix}=\begin{pmatrix}U_1^TU_1 & U_1^TU_1^\perp\\U_1^{\perp T}U_1 & U_1^{\perp T}U_1^\perp\end{pmatrix}$$

$$=U^TU=I$$

$$\Rightarrow U_1^TU_1^\perp=0,\ U_1^{\perp T}U_1^\perp=I,\ U_1^TU_1=I$$

If these two once more are divided, with

$$U_1 = \begin{pmatrix} U_{11} \\ U_{12} \end{pmatrix},\ U_1^{\perp} = \begin{pmatrix} U_{21} \\ U_{22} \end{pmatrix}$$

we have the following singular value decomposition of Z:

$$Z = \begin{pmatrix} Z_1 \\ Z_2 \end{pmatrix} = U\Sigma V^T = \begin{pmatrix} U_{11} & U_{12} \\ U_{21} & U_{22} \end{pmatrix} \begin{pmatrix} \Sigma_{11} & 0 \\ 0 & 0 \end{pmatrix} V^T$$

The matrices have the dimensions:

$$\Sigma_{11} \in \Re^{(2mr+n)\times(2mr+n)}$$
$$U_{11} \in \Re^{(mr+pr)\times(2mr+n)}$$
$$U_{12} \in \Re^{(mr+pr)\times(2pr-n)}$$
$$U_{21} \in \Re^{(mr+pr)\times(2mr+n)}$$
$$U_{22} \in \Re^{(mr+pr)\times(2pr-n)}$$

Since

$$\begin{pmatrix} U_{12} \\ U_{22} \end{pmatrix}^T \begin{pmatrix} U_{11} & U_{12} \\ U_{21} & U_{22} \end{pmatrix} \begin{pmatrix} \Sigma_{11} & 0 \\ 0 & 0 \end{pmatrix} = U_1^{\perp T} \begin{pmatrix} U_1 & U_1^{\perp} \end{pmatrix} = \begin{pmatrix} 0 & I \end{pmatrix} \begin{pmatrix} \Sigma_{11} & 0 \\ 0 & 0 \end{pmatrix} = 0$$

the relationship between Z_2 and Z_1 is the intersection of the row spaces

$$0 = \begin{pmatrix} U_{12} \\ U_{22} \end{pmatrix}^T \begin{pmatrix} Z_1 \\ Z_2 \end{pmatrix} \Leftrightarrow U_{12}^T Z_1 = -U_{22}^T Z_2$$

$U_{12}^T Z_1$ contains (2pr-n) row vectors, but only n of these are linearly independent. To determine the suitable row vectors the singular value decomposition of $U_{12}^T Z_1$ could be used,

$$\begin{aligned} U_{12}^T Z_1 &= U_{12}^T \begin{pmatrix} U_{11} & U_{12} \end{pmatrix} \begin{pmatrix} \Sigma_{11} & 0 \\ 0 & 0 \end{pmatrix} V^T \\ &= \begin{pmatrix} U_{12}^T U_{11} \Sigma_{11} & 0 \end{pmatrix} V^T \end{aligned}$$

but the singular value decomposition of just $U_{12}^T U_{11} \Sigma_{11}$ can be used instead, which with the orthogonal matrices U_n and $U_n^{\perp}$ gives

$$\begin{aligned} U_{12}^T U_{11} \Sigma_{11} &= \begin{pmatrix} U_n & U_n^{\perp} \end{pmatrix} \begin{pmatrix} \Sigma_n & 0 \\ 0 & 0 \end{pmatrix} V_n^T, \qquad U_n \in \Re^{(2pr-n)\times n} \\ &= \begin{pmatrix} U_n \Sigma_n V_n^T & 0 \end{pmatrix} V^T \\ &= U_n \begin{pmatrix} \Sigma_n & 0 \end{pmatrix} V_n^T V^T \end{aligned}$$

and $U_n^T U_n = I_{n\times n}$

$$U_n^T U_{12}^T Z_1 = \begin{pmatrix} \Sigma_n & 0 \end{pmatrix} V_n^T V^T$$

which is a basis of Z_1 and gives the following realisation of X_2

$$X_2 = U_n^T U_{12}^T Z_1, \qquad X_2 \in \Re^{n \times s}$$

The last step in the identification algorithm is to solve (for instance with the pseudo inverse) the overdetermined equations system and thus identifying the system matrices A, B, C and D

$$\begin{pmatrix} x_{k+j+1} & \cdots & x_{k+j+s-1} \\ y_{k+j} & \cdots & y_{k+j+s-2} \end{pmatrix} = \begin{pmatrix} A & B \\ C & D \end{pmatrix} \begin{pmatrix} x_{k+j} & \cdots & x_{k+j+s-2} \\ u_{k+j} & \cdots & u_{k+j+s-2} \end{pmatrix}$$

The residual sequences can then be determined as

$$\begin{pmatrix} \hat{w}_{k+j+1} & \cdots & \hat{w}_{k+j+s-1} \\ \hat{e}_{k+j} & \cdots & \hat{e}_{k+j+s-2} \end{pmatrix} = \begin{pmatrix} x_{k+j+1} & \cdots & x_{k+j+s-1} \\ y_{k+j} & \cdots & y_{k+j+s-2} \end{pmatrix} - \begin{pmatrix} \hat{A} & \hat{B} \\ \hat{C} & \hat{D} \end{pmatrix} \begin{pmatrix} x_{k+j} & \cdots & x_{k+j+s-2} \\ u_{k+j} & \cdots & u_{k+j+s-2} \end{pmatrix}$$

where $\hat{A}, \hat{B}, \hat{C}\ \hat{D}$ are the estimates of the system matrices and *e(k)* and *w(k)* are the residual sequences in output and state vector respectively.

Summarizing the algorithm, we have

1.Organise the input and output data in two Hankel matrices, Z_1 and Z_2, with relative timeshift of j=r

2.Compute the singular value decomposition of $Z = \begin{pmatrix} Z_1 \\ Z_2 \end{pmatrix}$

3.Compute the singular value decomposition of $U_{12}^T U_{11} \Sigma_{11}$

4.Compute $X_2 = U_n^T U_{12}^T Z_1$

5. Solve the overdetermined equations system $\begin{pmatrix} x_{k+r+1} & \cdots & x_{k+r+s-1} \\ y_{k+r} & \cdots & y_{k+r+s-2} \end{pmatrix} = \begin{pmatrix} A & B \\ C & D \end{pmatrix} \begin{pmatrix} x_{k+r} & \cdots & x_{k+r+s-2} \\ u_{k+r} & \cdots & u_{k+r+s-2} \end{pmatrix}$

The above algorithm requires knowledge of the system order. In order to determine the correct (minimal) system order the following solution has been proposed [Moonen et al 89].

$$Z = \begin{pmatrix} Y_h \\ U_h \end{pmatrix}$$

$$\begin{aligned} rank\, Z &= rank\, U_h + rank\, X \\ &= mr + n \end{aligned}$$

The requirement on the input matrix is that it has got full rank - i.e. persistent excitation of at least order r exists.

2.3 Simulations

The identification algorithms were tested on randomly generated systems created with the Matlab-routine *drmodel*. Systems of different order in state-space representation with one input and six to nine outputs were identified. Both disturbed (white noise where added to all the outputs) and undisturbed systems were generated.
At first the system order algorithm were used to find the minimal system order. In the deterministic (no disturbances) case the correct order was determined, but for the disturbed systems the algorithm did not terminate at the correct order - in fact, it did never terminate. Even a very small disturbance of 1% (i.e. a noise-signal ratio of 0.01) in the output resulted in failure.
The deterministic systems were always correctly identified, i.e. the system poles were found and the residuals were all zero.
The disturbed systems were correctly identified unless the noise-signal ratio was too high. A system of sixth order with a noise-signal ratio of 0.10 is below used as an example. The residuals in output and states (i.e. e(k) and w(k)) were analysed with four statistical tests, the Kolmogorov-Smirnov normal distribution test and three chi-2 tests: zero crossing test, auto correlation test and cross correlation test all with an confidence interval of 95% [Johansson 93]. The result is shown in table 2.1.

Test	e(1)	e(2)	e(3)	e(4)	e(5)	e(6)	w(1)	w(2)	w(3)	w(4)	w(5)	w(6)
Norm	*	*	*	*	*	*	*	*	*	*	*	*
Zero	*	*	*	*	N/168	*	*	*	*	*	N/171	*
Auto	*	*	*	*	N/80.4	*	*	*	N/83.3	N/142	N/88.4	N/77.1
Cross	*	*	*	*	N/69.2	N/69.1	*	N/99.5	*	N/103	N/123	N/75.8

Table 2.1 * denotes Test passed, N test not passed and the test value. In the zero crossing test a number within 133- 166 is accepted and in the auto-cross correlation tests the limit is 67.5, for 95% confidence interval.

After the statistical tests a cross validation and a deterministic simulation were made, the results for output 1 are shown in Figure 2.1. The system are correctly identified both in gain and dynamics, but there is a tendency to incorporate the disturbances in the model, on the whole the system behaviour is well reproduced and predicted. The input signal used in the cross validation were data 300 points after the input sequence used for the identification. The other outputs show a similar behaviour. The simulations of the systems with no disturbnce in the outputs are very well identified, which the theory also guarantees. In the disturbed cases all the poles are not correctly identified, but the results of the deterministic simulations and cross validations show that the identified systems behave like the true systems. The residuals of w(k) are not as "white" as the e(k) residuals, this might be an indication that these still have some remaining information about the system dynamics. However, the test quantities are (with the ex-ception of w(4) and w(5)) close to the acceptance limit and again the identified system follows the real output values well in the cross validations and the deterministic simulations. It should be noted that the residual tests for n=5 and n=7, i.e., for system orders lower and higher than the correct one, gave a similar result in w(k) as for n=6, but the e(k) residuals were worse in both the non correct cases.

The conclusions drawn from the result of the simulations are that the system order algorithm does not function for real systems, but the subspace algorithm identifies these systems well, although there are some peculiarities about the residual sequence w(k).

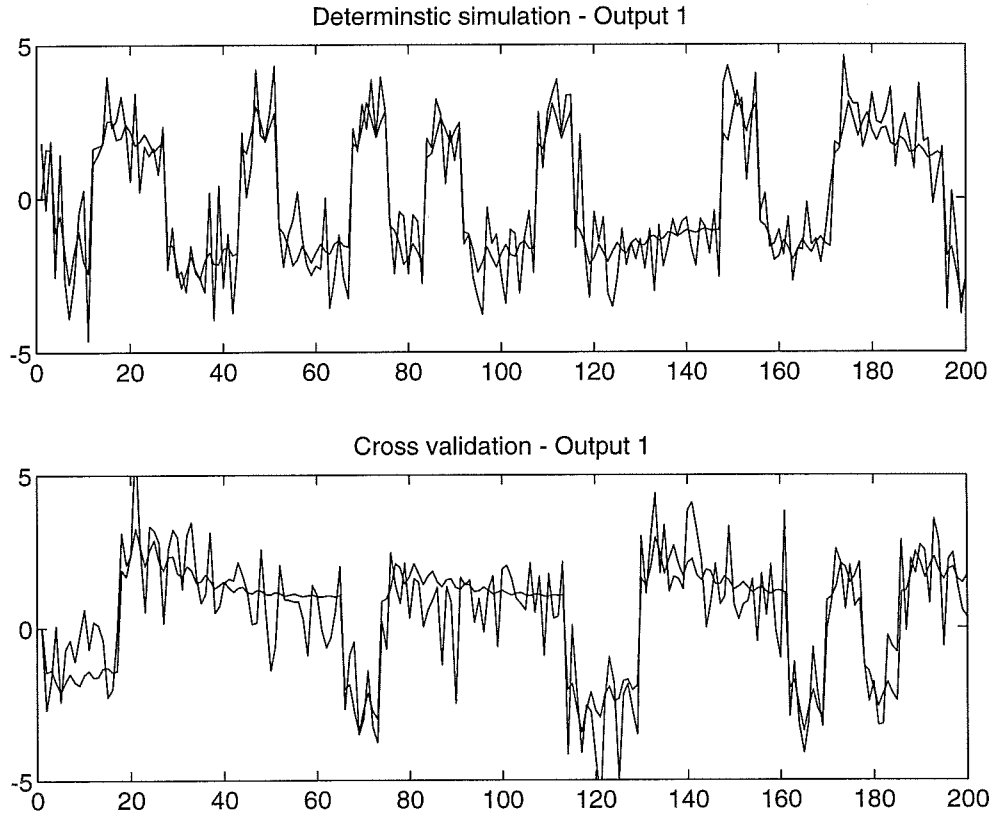

Figure 2.1 Deterministic simulation and cross validation of output 1. Dashed line - simulated output, solid line - measured output.

3 Materials and methods

The experimental setup and the above described algorithm were first tested on two female test subjects (55 and 26 years old). After the analysis of the two pilot tests, a series of seven subjects were tested. The following equipment were used:

-Force platform— a tool for measuring of contact forces. The alteration of the resistances in six ring sensors due to pressure from the feet are used to determine a six-axis force state (three torques and three forces). The platform was designed and constructed at the department of Solid Mechanics, Lund Institute of Technology.

-Selspot— Position monitoring equipment consisting of a controller unit, two CCD cameras and one or two LEDs (Light Emitting Diode).The Selspot system is manufactured by Selective Electronic Co AB Sweden.

-Vibrator— a revolving DC-motor equipped with a eccentric weight at one end. The vibration frequency was 60 Hz and the amplitude was 0.4 mm (light vibrator) or 1.0 mm (heavy vibrator).

-AD/DA converter, AI-MIO-16L/9

-PC— Hewlett Packard 486, DX-2 66 Mhz, equipped with the software Postcon and Matlab.

The test subject was placed on the platform with feet spread (angle 30 deg) and with vibrators strapped to the calf muscles on each leg. One LED was placed on the hipbone, if the second LED was used it was placed on the thigh approximately 20 cm down from the first diode. The two cameras were placed 120 cm away from the subject and their lines of convergence created an angle of 20 deg. The distance between the center of the camera lenses was 63 cm.
The measurement started with a resting phase of 30 seconds, thereafter vibrations were generated to induce sway by the subject, the sway is due to the erroneous proprioceptive information. This period lasted 205 seconds. The measurement process were controlled by the software Postcon (written in LabView by Per Anders Fransson ENT Department Lund University Hospital). The sample rate was 10 Hz.
As input signal a PRBS (Pseudo Random Binary Sequence) was used and nine (one diode) respectively twelve outputs were measured. Six of these were the three torques (Mx, My and Mz), the two shear forces (Fx and Fy) and the weight (Fz) from the force platform, the other were the x-, y- and z-coordinates of the diode(s). In the analysis three of the outputs (Mz, Fz and z) were omitted.

The identification method followed the following scheme:

1. The data were detrended and identified with the matlab macros *sub1* (one diode) and *sub2* (two diodes). s were chosen to 300 (which means that approximately 30 seconds of measurement data were analysed), and r were set to be equal n (the system order). The analysis started 75 seconds after the first stimulation, to avoid the chaotic behaviour at the test start.

2. A balanced realisation were found, and the breakpoints of the singular values in the gramian decided which system order, that was chosen.

3. The residuals were computed and analysed with three statistical chi-2 tests [Johansson 93]; zero crossing test, auto correlation test and cross correlation test (residual-input).

4. A balanced model reduction was carried out.

5. Deterministic simulations were made, i.e. the identified system was simulated and compared to measured data.

6. Cross validation was made, the simulated system were driven with input data 30 seconds after the sequence used as input in the identification.

After the pilot tests a study with eight subjects, four females and three males (mean age 24, range 23-26 years), were made, see table 3.1. None of the subjects had any history of vertigo, central nervous disorder, ear disease or injury to the lower extremities, and no subject was on any form of medication or had consumed alcohol the last 24 hours.

	Age	Sex
Subject 1	24 years	Male
Subject 2	24 years	Male
Subject 3	23 years	Male
Subject 4	26 years	Female
Subject 5	23 years	Female
Subject 6	24 years	Female
Subject 7	24 years	Female

Table 3.1 Test subjects

The same equipment and experimental set-up as in the pilot tests were used. The subjects were subjected to four tests; light vibrators and two diodes with eyes closed (test 1), light vibrators and two diodes with eyes open (test 2), heavy vibrators and two diodes with eyes closed (test 3) and heavy vibrators and two diodes with eyes open (test 4).
The data was analysed using the Matlab macro *sspace*, three periods each of 30 seconds (s=300) were analysed with a system order n=6 for the case of light vibrators and n=8 for the case of the heavy. The model order was found with balanced model reduction and all states lesser than 10% of the largest singular value were taken out of the model. One force (Fy), the Mx-torque and the two y-coordinates y1 and y2 were considered. The system matrices were identified and the pole distribution were computed. The systems were deterministic simulated and finally cross validated.

4 Results

The results of the pilot tests are found in 4.1 and the results of the main study in section 4.3, this chapter ends with a coloured noise approach to model the residuals w(k) and e(k).

4.1 Pilot tests

4.1.1 Results of identification with nine outputs

The coherence between stimulus and response was tested. Outputs Mx, Fy and y showed a good coherence for lower frequencies (f<2 Hz) but a non acceptable coherence for higher frequencies, the low coherence for higher frequencies is a result of the body's inability to sway with a higher frequency than around 2 Hz. No coherence between the input (PRBS-signal) and the other outputs were not found. The computed coherence spectra for Fy, Mx, y and My can be found in Figure 4.1. The 2-norm of each output also shows that Mx and Fy are the most alternating outputs among the force platform outputs and the same is true for y among the Selspot outputs. Mz and z hardly change at all, i.e., there is no twisting movement or up and down movement. Mx, Fy and y correspond linearly to the input, the other outputs are either nonlinear in their response or very disturbed.
The coherence analysis for the case of heavy vibrators shows a similar result as for the light, although the coherence is slightly worse for the heavy vibrators. Fy, Mx and y have a good coherence for frequencies lower than 2 Hz. All the other outputs have a nonlinear response to the stimulation or are to small/disturbed. The coherence spectra for some outputs are shown in Figure 4.2.

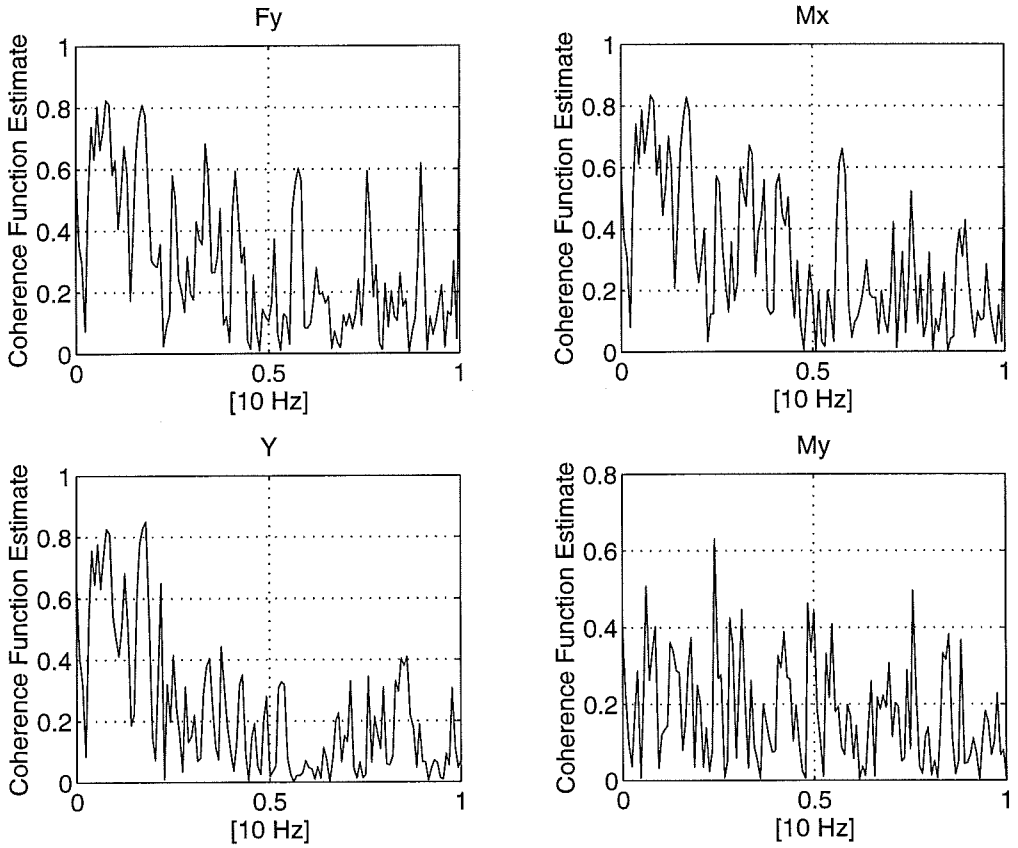

Figure 4.1 Quadratic coherence spectra between input and outputs Fy, Mx, Y and My, light vibrator test.

Output	Fx	Fy	Fz	Mx	My	Mz	y	x	z
2-Norm	0.302	0.596	0.491	1.0	0.465	0.015	0.247	0.188	0.034

Table 4.1 Normalised 2-norms of all outputs, light vibrators.

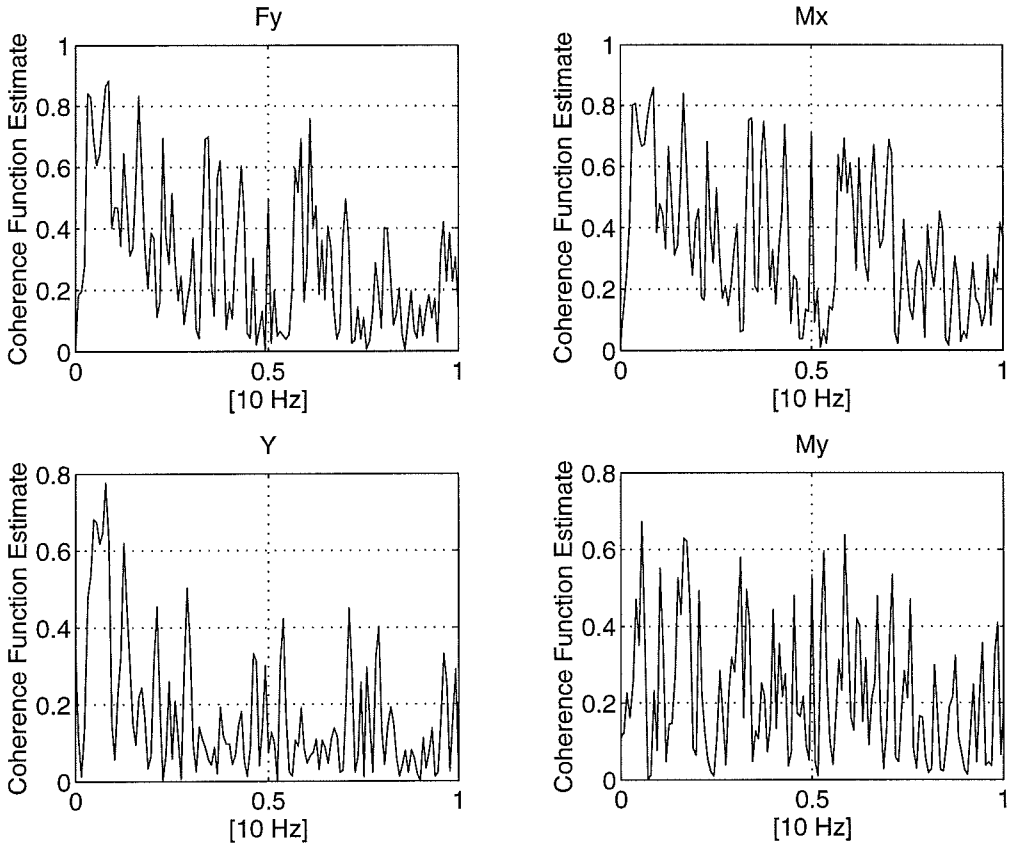

Figure 4.2 Quadratic coherence spectra for outputs Fy, Mx, Y and My, heavy vibrator test.

In the light vibrator stimulation case Mx and y are very well correlated, with a correlation (regression) coefficient in the least square sense of -0.9797. The Mx vs. Y plot (Figure 4.3) between the two clearly shows this fact. The subject used the above explained ankle strategy, which means the response of the body to a small disturbance can be modelled as an inverted pendulum. The result are similar for heavy vibrations, although Mx and y are to a lesser degree correlated to each other, with a correlation (regression) coefficient of -0.8340. The larger disturbance causes a more complex movement pattern of the body than a small one for this subject.

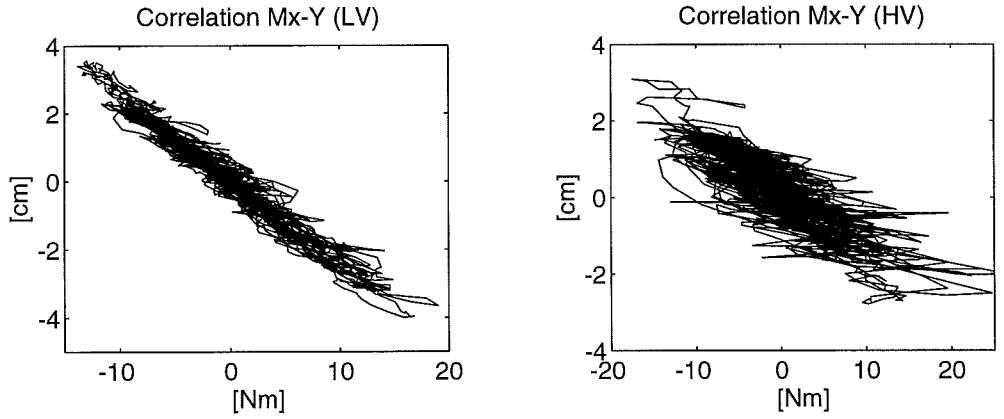

Figure 4.3 Correlation between Mx and Y. As can be seen in the plots there is a strong linear dependence between the two outputs, for the light vibrators (left) the correlation coefficient in the least squares sense is -0.9797 and for the heavy (right) -0.834.

The results of an identification with all nine outputs for the case of weak amplitude stimulation are now shown. The normalised singular values of the gramian for a fifteen order system can be found in Figure 4.4 together with different pole configurations. The singular-value sequence has got two clear breakpoints at index 4 and at index 9, which indicates a model order of 4 or 9. All singular values with indices higher than four are lower than 0.1, a sufficient model order therefore is 4, i.e. the first breakpoint should be chosen for the balanced model reduction. The residual analysis however clearly contradicts this result as can be seen in Figure 4.5, the residual test values show that a model order of n=6 cannot be accepted. Higher model orders pass the cross correlation tests (no unidentified feedback exists in the system), but no order pass the auto correlation test (which means that the residuals are not white noise sequences). Not many of the residuals pass this test but for n=9 and up the residuals in the forces and the Mx-torque are acceptable. All the residuals in the Selspot outputs fail the test extensively. These residuals are oscillating and cannot be considered as white even for a very high system order as n=15. It is not clear how to choose an appropriate model order.

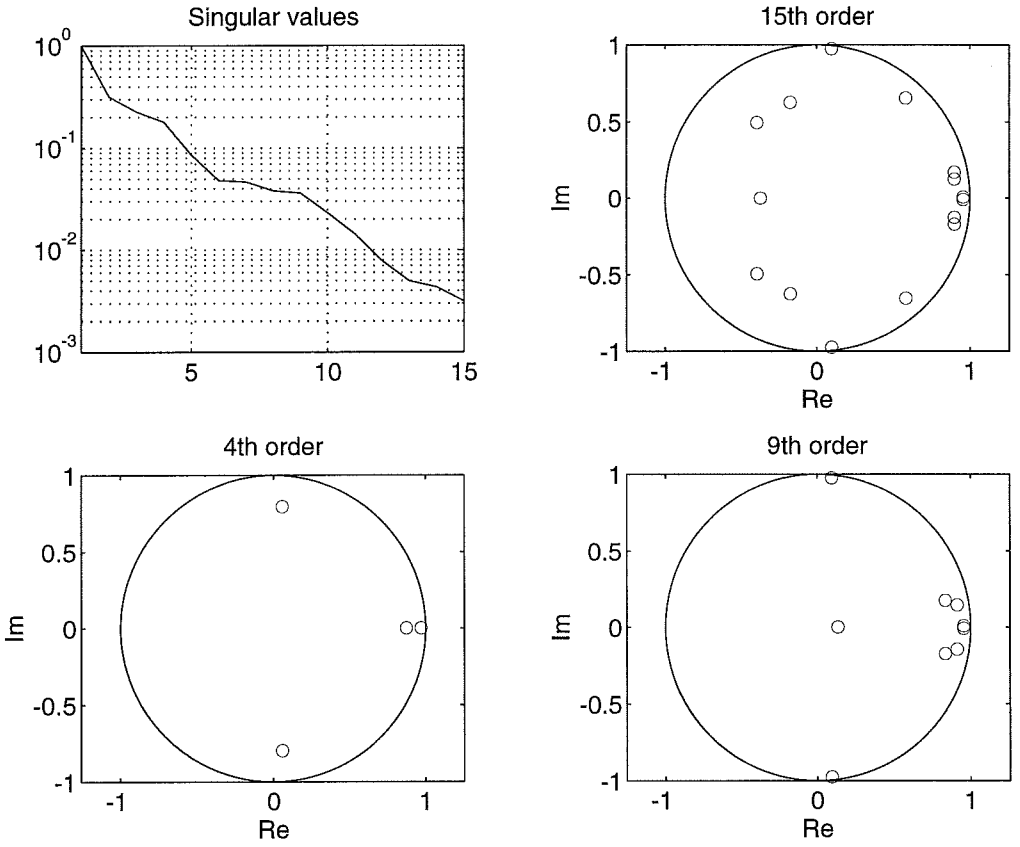

Figure 4.4 Singular values and pole distributions, light vibrator test.

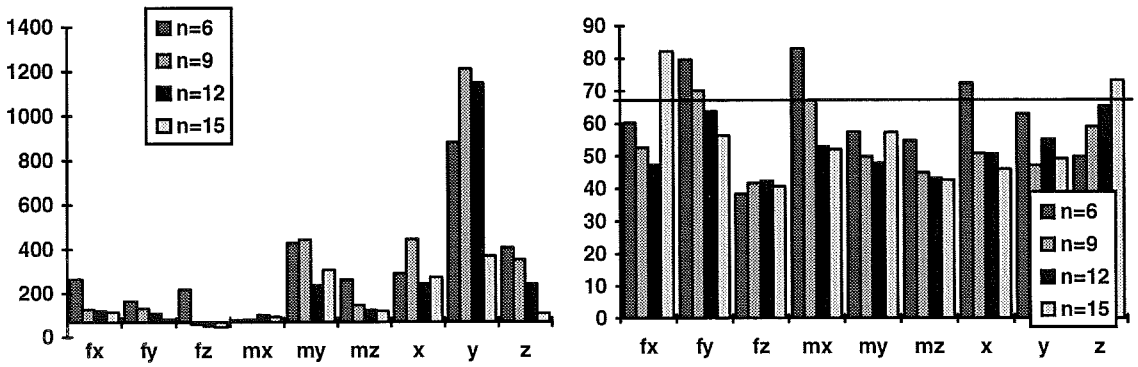

Figure 4.5 The left diagram show the test values for the autocorrelation test and the right diagram the values for the cross correlation. In the left diagram test passed is indicated by an inverted box and in the right the drawn line sets the limit for test passed (67.5 for 95% confidence interval).

The results of a total residual analysis (w(k) as well as e(k)) for n=15 is shown in Table 4.2 and Figure 4.6. The w(k) residuals do not pass the auto correlation test, which should mean that the model order is too low. One possible interpretation is that the method tries to model not only the real system dynamics but also the noise, thus that the true model order is "hidden" in the disturbances. A new method approach with coloured noise might give a better result, such an approach is found in *4.4 Stochastic realisation of residuals.* The simulated data did also exhibit this behaviour in the w(k) residuals.

	Fx	Fy	Fz	Mx	My	Mz	y	x	z
Auto	N/115	N/82.2	*	*	N/307	N/119	N/273	N/369	N/107
Cross	N/82.2	*	*	*	*	*	*	N/73.4	*
Zero	*	*	*	N/120	N/96	N/116	N/77	N/99	N/84

Table 4.2 Residual analysis for n=15. * denotes test passed, N test not passed and the test value. In the zero crossing test a number within 133-166 is accepted and in the auto- and cross correlation tests the limit is 67.5 (95% confidence interval).

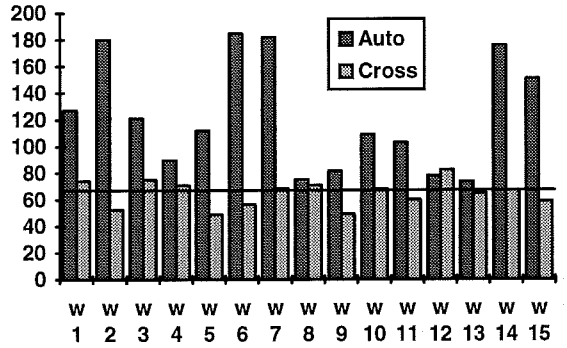

Figure 4.6
Results from auto- and cross correlation tests for residuals w(k). The line sets the limit for test passed (95% confidence interval).

The deterministic simulation of this fifteen order system are shown in Figure 4.7 and Figure 4.8. Outputs Fy, Mx and y are well simulated and Fx and My are acceptably simulated, but there are errors in gain and faster dynamics for all outputs. The vertical force, Fz, is a very large and oscillating output, which the model cannot simulate. Fz is the most amplified output in the force transformation (the voltage to force factor is around 730), and the maximum change in Fz corresponds to a change of 1.0 kg in weight. It might be the case that disturbances are amplified in the transformation. This output should be omitted from the analysis. The Selspot outputs x and z are together with Mz much smaller than the other and at least Mz and z can be taken out of the model, since they do not contribute to the system behaviour. The oscillation in z and x are probably due to noise or the use of a median filter in the computation of the coordinates. Note the discrepancies in all outputs around k=150, this is probably due to a long period (six seconds) without any stimulation, which makes the movements of the subject impossible to trace to the stimulation.

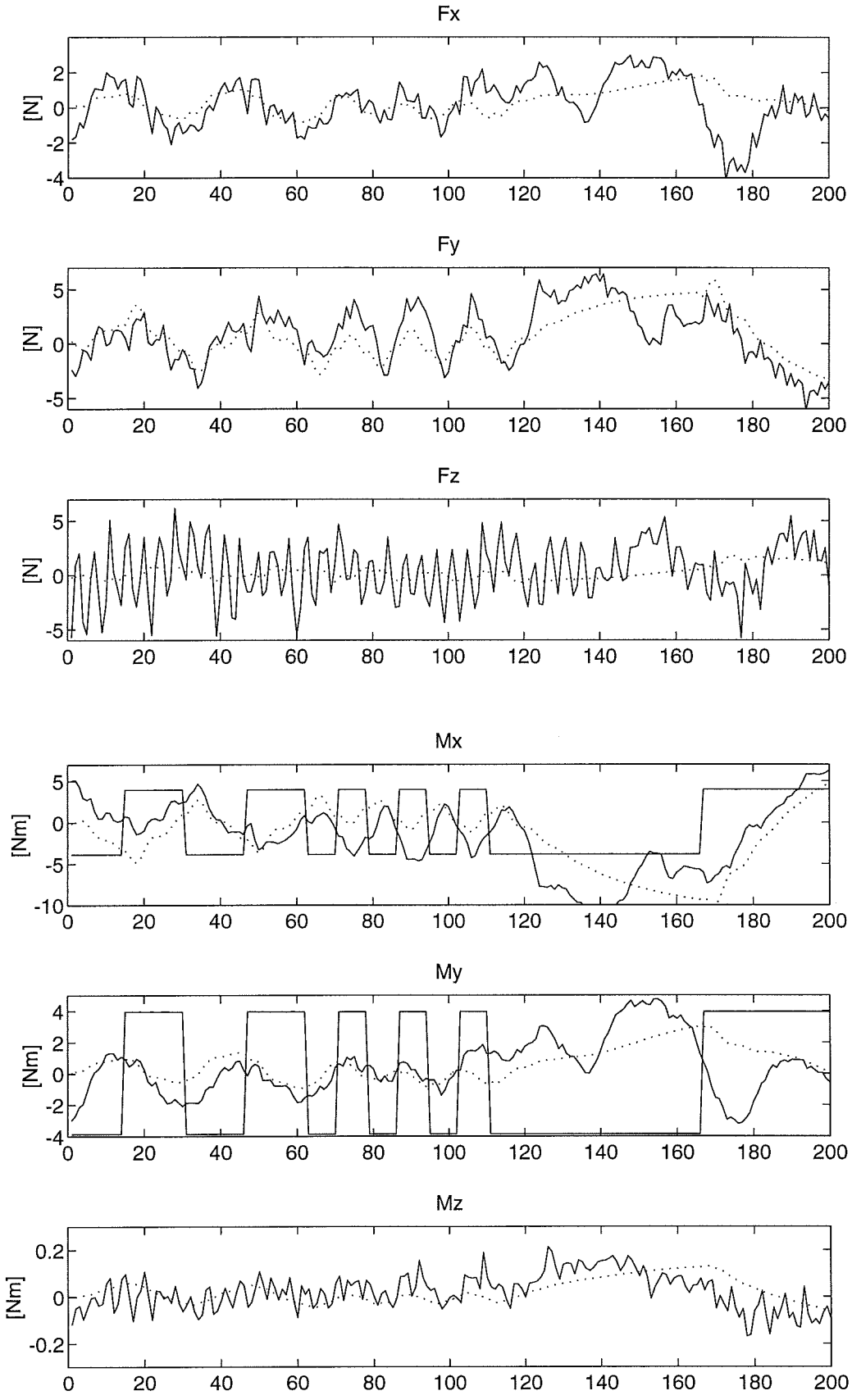

Figure 4.7 Deterministic simulation of outputs Fx, Fy, Fz, Mx, My and Mz. Dotted line - simulated output, solid line - measured output.

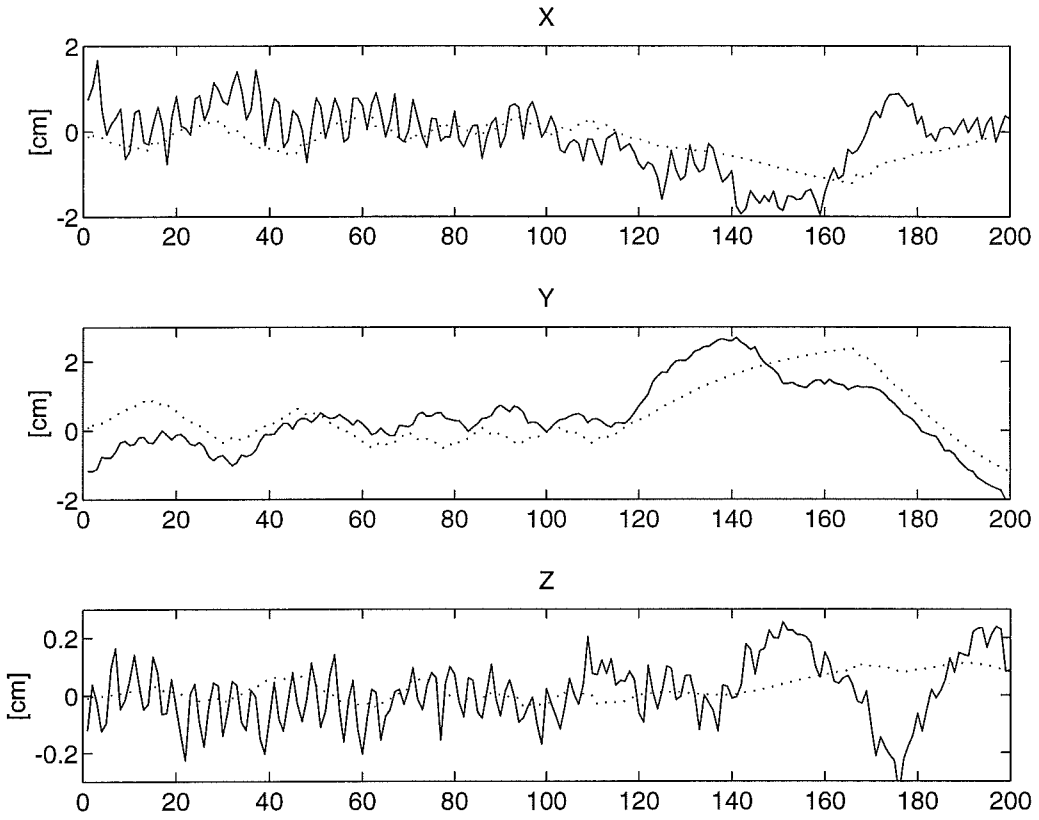

Figure 4.8 Deterministic simulation of outputs X, Y and Z. Dotted line - simulated output, solid line - measured output.

The low coherence between input and outputs Fz, Mz and z depends on their high noise-signal ratio, which is seen in the deterministic simulations. The explanations for output Fx, My and y are found in the cross validations. The data used in the cross validations were picked 30 seconds after the identification period's end. The cross validations for Fy, Mx and y (the results of Mx can be seen in Figure 4.9) show that the model can predict these outputs' behaviour well, although there is an offset for values further away in time, which might correspond to a change in the subjects reaction to the stimulation. The system is slightly time variant for these outputs. The cross validations of Fx, My and x give a very bad result. This inability to predict Fx, My and x as good as the other variables depends on the nature of the outputs. My is a measurement of the lateral "sway" and can be induced either way (to the left or to the right) by the stimulation. In reality the initial direction might well be random or chaotic. During the measurement period used in the identification the stimulation happens to induce sway mostly in one direction, but this is not valid for the whole measurement period. The response to the stimulus is nonlinear (compare with the coherence analysis), My, Fx and x (the latter are coupled to the former by the laws of mechanics) should therefore not be considered in the analysis. But lateral sway is induced by calf stimulation.

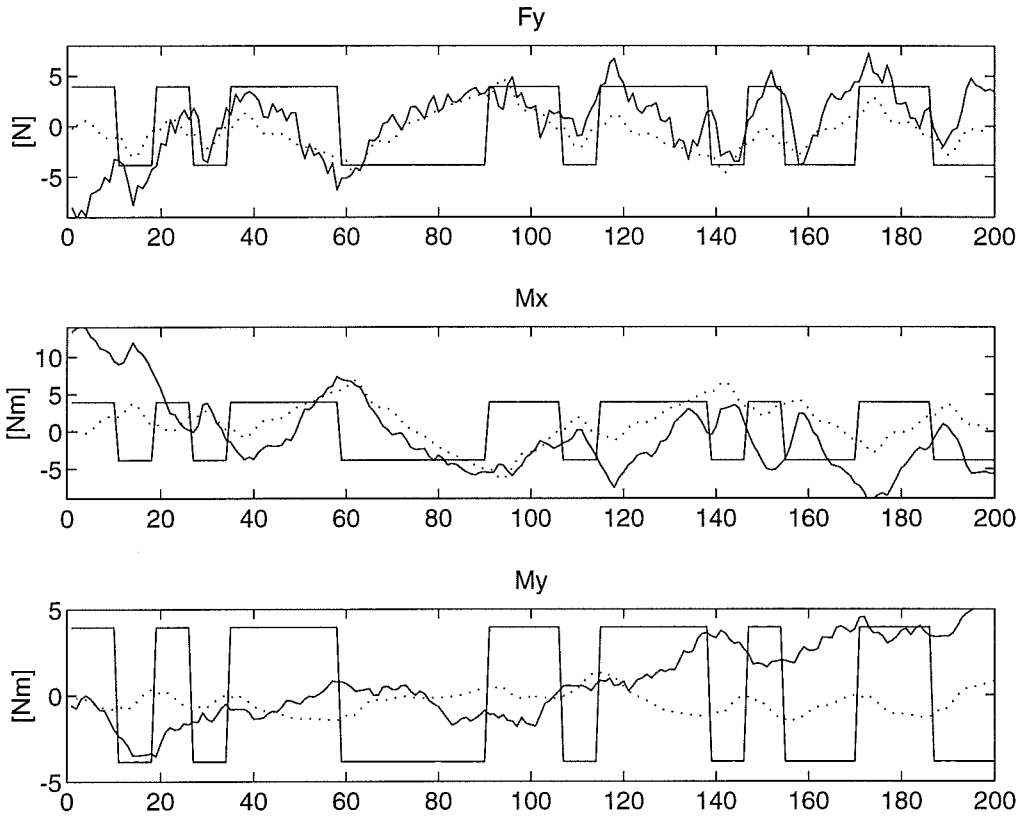

Figure 4.9 Cross validation of Mx and Y. Dotted line - simulated output, solid line - measured output. The PRBS-signal is also plotted.

To find the correct model order two balanced model reductions were computed, the first reduced the model order from 15 to n=4, the second to n=9. The pole configuration (Figure 4.4) of the original system and for the ninth order system show two integral poles at z=1, two very oscillating poles on the unit circle and a cluster of lightly damped poles close to z=1. Both deterministic simulation and cross validation (Figure 4.10) give better results for the higher order.

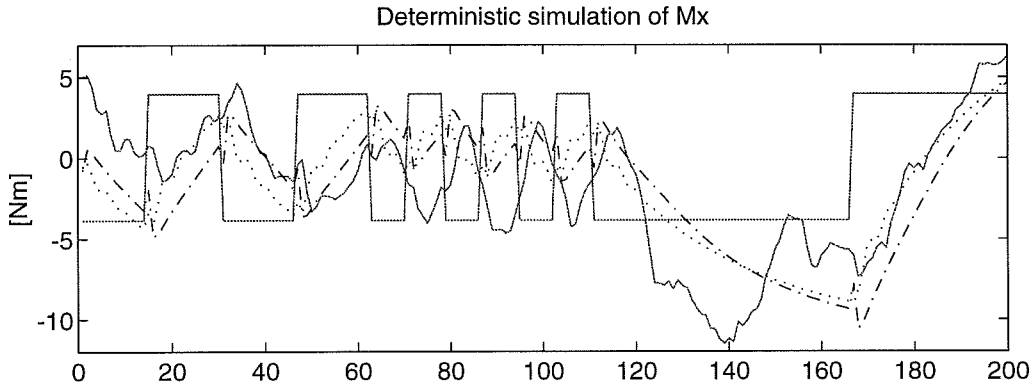

Figure 4.10 Deterministic simulation of Mx for systems after balanced model reduction. Dotted line - simulated output for n=4, dash-dotted line - simulated output for n=9, solid line - measured output.

4.1.2 Results of identification with three outputs

Results from identification with 9 outputs show that only Fy, Mx and y are relevant for both the type of stimulation. In this section the results from an identification with just these three outputs are shown. A sequence somewhat prior to the one above was used, to avoid the long period without any stimulation.
The singular values of a high order system gives a model order of n=6 for light vibrator case. As can be seen in Figure 4.11 the diagram of normalised singular values have got other breakpoints than at number six, but all singular values with an index higher than six is lower than 0.1. The pole distribution for a system with just three outputs are a bit different than with nine (as can be expected because another identification period was used), but still there are poles close to z=1 and oscillating poles near the unit circle. The singular-values diagram for heavy vibration of a 21 order system does not give a clear choice of new model order. There are breakpoints at n=9, n=13 and n=16, since all singular values with indices larger than eleven are smaller than 0.1, n=13 is a reasonable choice. The higher model order for the case of heavy vibrators makes sense as the correlation between Mx and y was lesser. The model of the inverted pendulum cannot describe the body's response to the stimulus perfectly. Note the different result in the main study. Singular values are shown in figure 4.11.

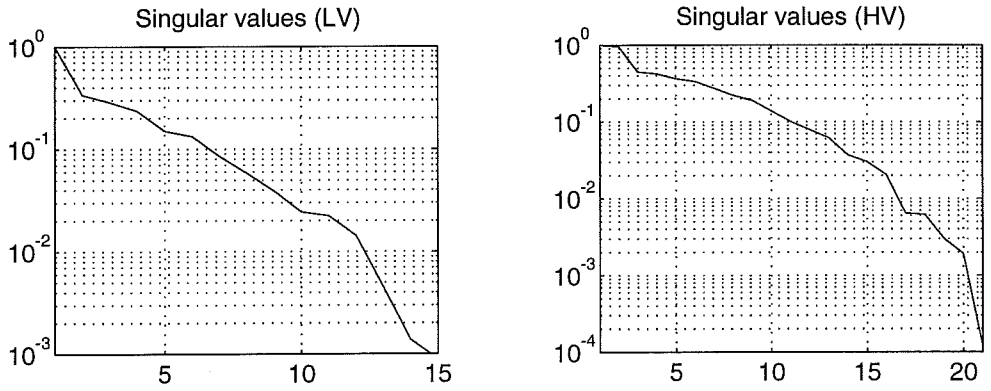

Figure 4.11 Singular values for light (left plot) and heavy vibrators (right plot). A system order of 15 respectively 21 were used.

Again the residual analysis gives another result. The residuals (in the outputs) of model order n=4 to n=18 were tested. All residuals pass the cross correlation test and almost all pass the zero crossing test, but none passes the auto correlation test. The differences between Selspot data and platform data, which were found in the section above, has vanished. The residuals do not show a clear decreasing pattern in test value with higher model order, instead the values sometimes drop and sometimes rise. According to this test a correct model order should be n=15 or n=16 (taking the minimum of all three residuals, see Figure 4.12). The variances of the residuals, however, drop quickly with higher model order to stabilise around n=6. This indicates a model order of six.

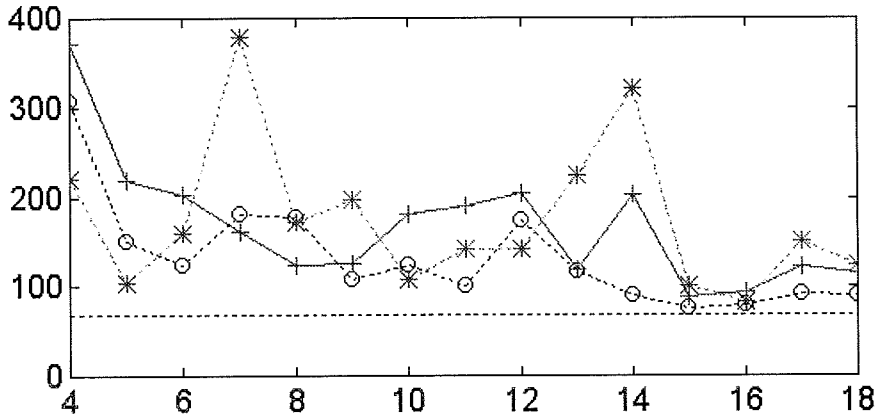

Figure 4.12 Autocorrelation test values for different model orders for light vibrators, o - Fy, + - Mx and * - y. The dashed line indicates the limit for 95% confidence interval, under white-noise model assumption.

Also the residual analysis of the heavy vibrator test does not give a clear result. The residuals in y are very large and fail by very much in all tests (especially in the autocorrelation and zero crossings tests, the test values of the cross correlation test are close to the acceptance limit). The other two (output) residuals both pass the auto-correlation test for a nineteenth order model. The cross correlation test is passed by the Mx and Fy residual for n=15 (they are rather close to the limit already for a sixth order model) and they pass the zero crossing test for all orders. As for the case with light vibrators the residuals do not exhibit a clear pattern. The behaviour in the auto-correlation test for Fy and Mx are shown in Figure 4.13. Notice the rolling pattern, the residuals in x are much larger with values around 500 and therefore not shown in the Figure 4.13, but they also have these changes in test values.

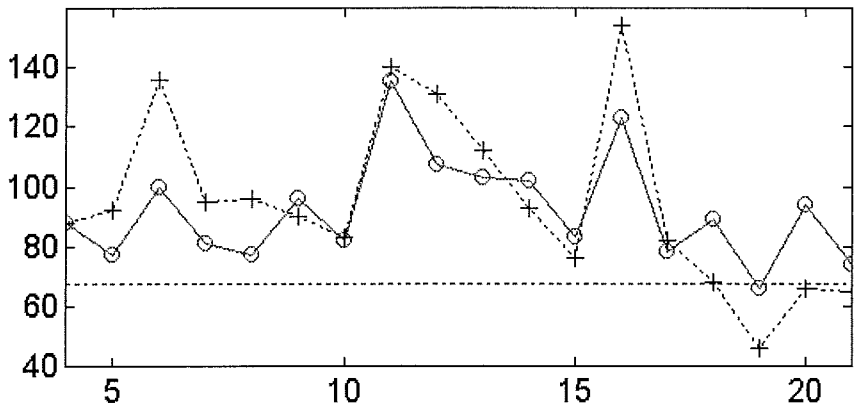

Figure 4.13 Autocorrelation test values for different model orders for heavy vibrators, o - Fy, + - Mx and * - y. The dashed line indicates the limit for 95% confidence interval, under white-noise model assumption.

Deterministic simulations and cross validation for n=6 and n=15 show that the higher model order does not give a much better result (Figure 4.15). The differences between n=6 and n=15 are very small both for the deterministic simulations and for the cross validations. The slower dynamics are acceptably identified, but there are errors in gain and in the faster dynamics. The cross validation shows that the system is slightly time variant.
The system for n=6 has the following poles, two poles close to z=1, which gives an integral part, one pole close to z=0, the time delay(?), and two well damped imaginary poles. The last pole is situated on the negative real axis and lacks a time continous model of the same order. See Figure 4.14.

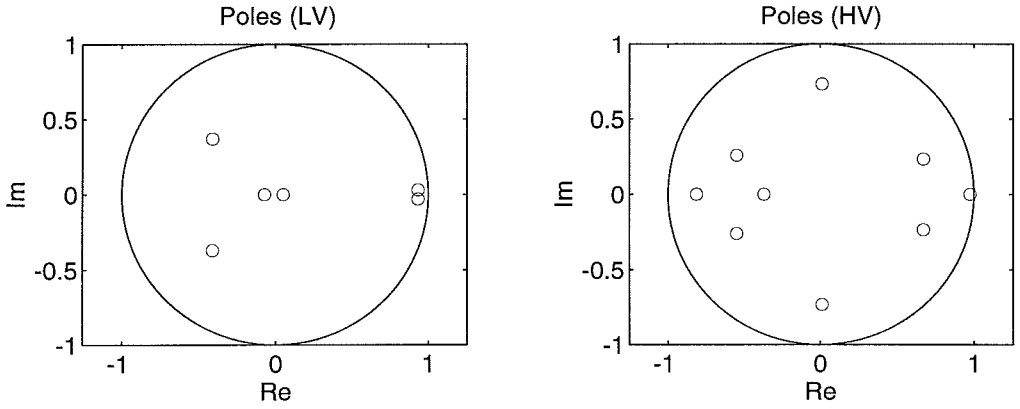

Figure 4.14 Pole distributions for both pilot tests, notice the artefact poles on the negative real axis in both tests.

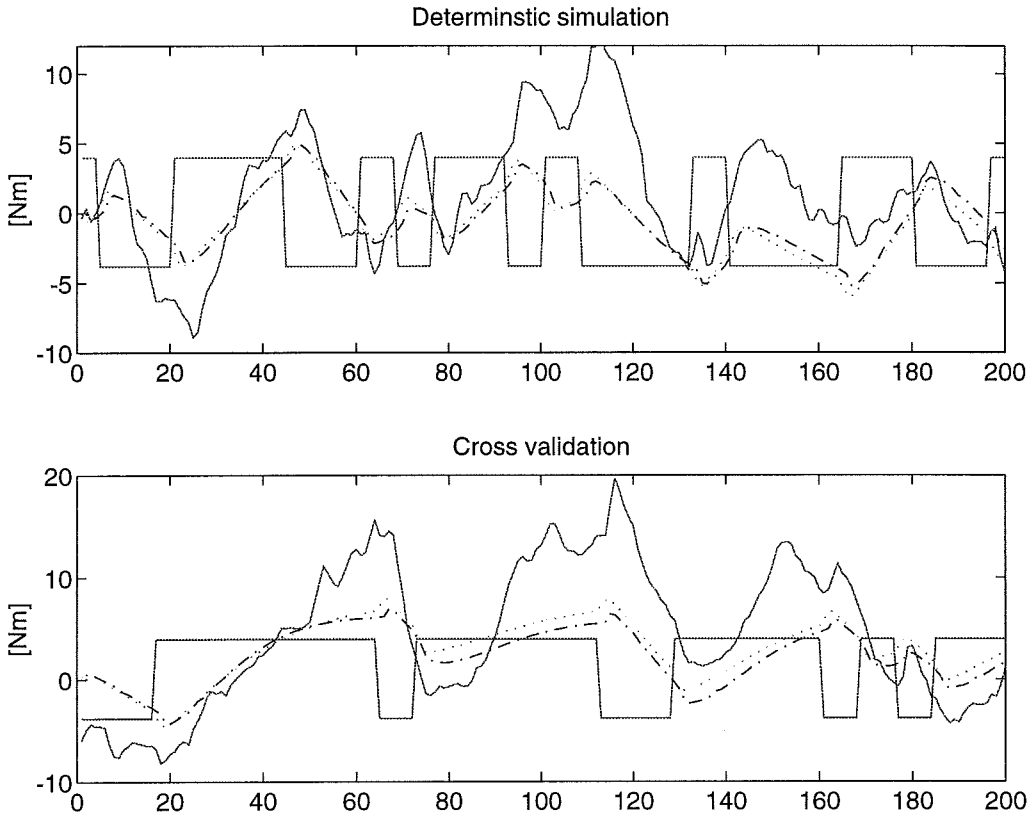

Figure 4.15 Deterministic simulation and cross validation of Mx for n=6 and n=15, light vibrators. Dotted line - simulated output for n=6, dash-dotted line - simulated output for n=15, solid line - measured output.

To find a suitable model order both n=9, n=13 and n=16 were simulated. In Figure 4.16 the deterministic simulation and cross validation for Mx is shown. The other two output have a similar behaviour. As can be noted in the deterministic simulation the simulated data independent of model order cannot recreate the fast dynamics and tend to have a to low gain. The ninth-order system performs slightly worse than the others, but all the orders are quite equal. The simulation differs more from the measured data than the case was in the light vibrator test. The same is true for the cross validation, where again the ninth-order system is worse than the others. None of the systems give a very good result in this test, they manage to predict the general slow dynamic rather well, but gain and the fast changes are not caught. It seems that a system order of 9 should be enough. The difficulties to find the correct model order are once again shown. Since none of the methods (especially the residual test method) give any easy interpreted result, it is hard to say anything about the optimal model order. The pole distribution (n=9) are quite similar to the one for light vibrators, we have poles close to z=1, poles close to the unit circle, one pole close to zero and one non physical pole on the negative real axis, although the latter is somewhat more dominating than in the other case. See Figure 4.14.

The step and impulse responses are shown in Figure 4.17 for the both pilot tests. The rise time is 4.6 seconds and the gain 1.86. What cannot be seen in the figure is a very small overshoot around k=80 for the step response. The time it takes for the impulse response to fade out is 7.5 seconds. The rise time is 1.7 seconds and the gain is 1.05. The time for the impulse response to die out is 3.0 seconds.

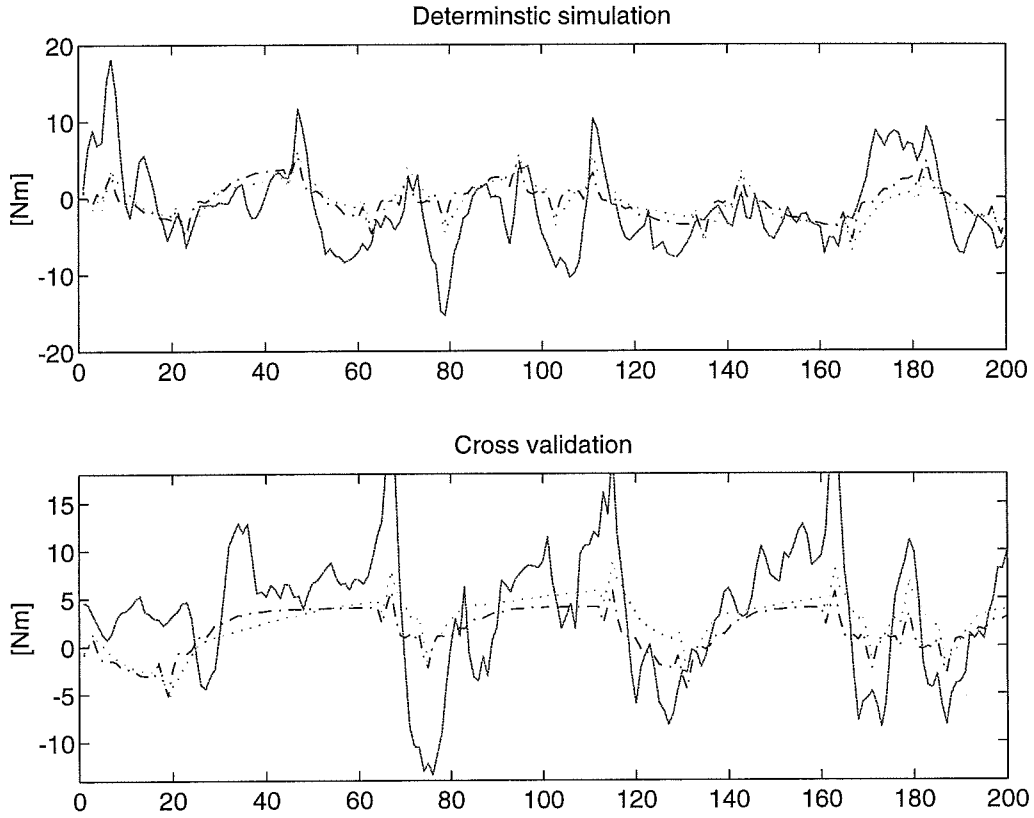

Figure 4.16 Deterministic simulation and cross validations of Mx for n=9 and n=19, heavy vibrators. Dotted line - simulated output for n=6, dash-dotted line - simulated output for n=15, solid line - measured output.

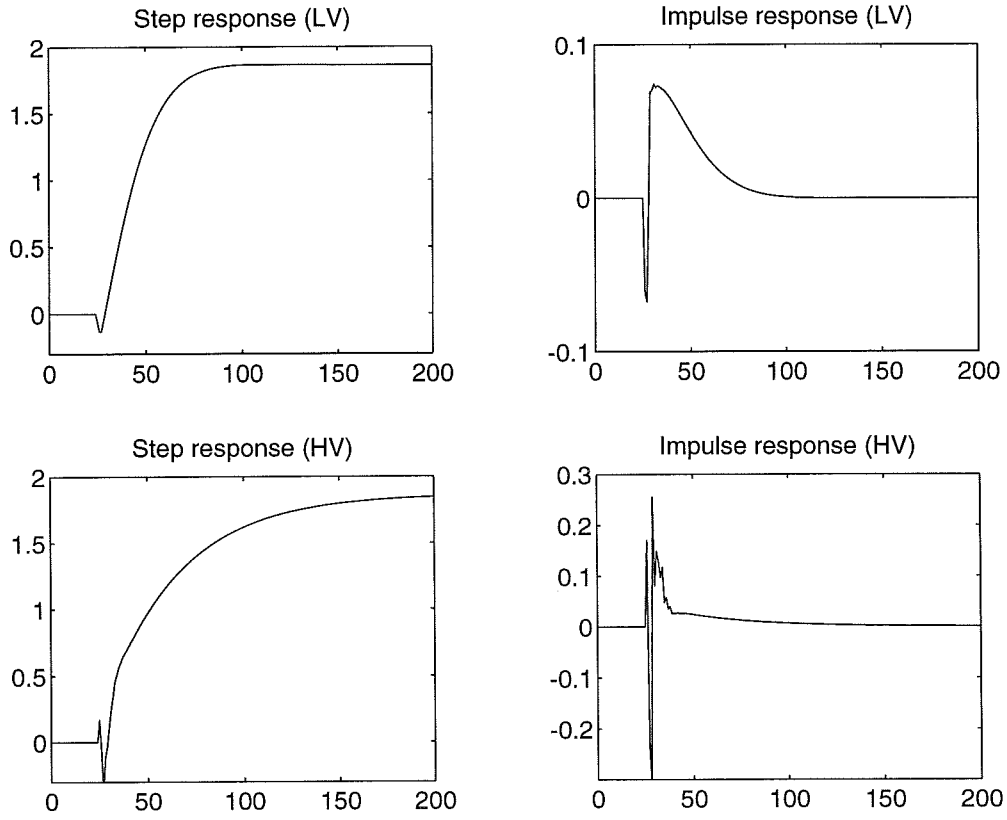

Figure 4.17 Step and impulse responses for both pilot tests.

4.2 Choice of r

Different values of r (block row number) were tested for small amplitude stimulation with three outputs and n=6. The pole distribution is altered with the r value, the poles close to z=1 remain but the other poles move around (see Figure 4.18). The identified systems for r=n+1 to r=n+5 are not correctly simulated in the deterministic simulation. The time delay is not found and the gain is even more wrong than for r=n. For r=n+6 the time delay and the gain again equals r=n (see Figure 4.19), higher values of r do not give a better result. The deterministic simulation and cross validation for r=n+6 give an equal result as for r=n. The optimal value of r is either r=n or r>n+5. The lower value lessens the computational effort and should therefore be chosen.

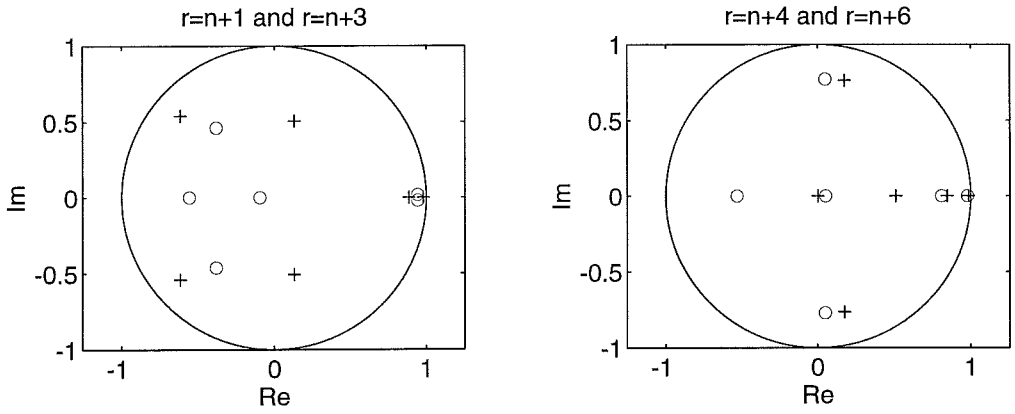

Figure 4.18 Pole distributions for different r-values. o - poles of r=n+1 (left plot) and r=n+4 (right plot), + - poles of r=n+3 (left plot) and r=n+6 (right plot).

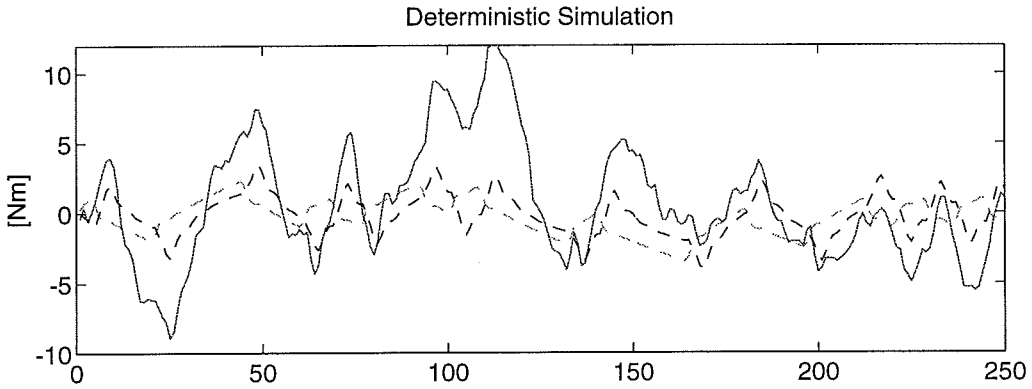

Figure 4.19 Simulation of Mx with r=n+3 and r=n+6 for a sixth-order system. Dashed line - simulated output of r=n+3, dash-dotted line - simulated output of r=n+6, solid line - measured output.

4.3 Results of main study

In table 4.4 the correlation coefficients between Mx and y (just y means coordinate of body mass centre, which is equal to y1) for all four tests and all test subjects are shown, notice that subject 2 did not take part in test 4. The coefficients are all around 0.9, which means there is a strong linear dependence between Mx and y for all subjects and tests. There is also a strong correlation between the shear force Fy and Mx, and there is to a lesser degree a correlation between y and Fy, note the negative coefficient does not mean negative correlation, but a negative regression coefficient. The correlation between Mx and y is higher for all subjects with eyes open than eyes closed, except for subject 1 (light and heavy vibrators) and subject 7 (just light vibrators). The correlation between Mx and Fy for the case of light vibrators is lower for 5 subjects with eyes closed than eyes open, with the heavy vibrators 2 subjects have lower correlation with eyes closed than eyes open. See Tables 4.4-4.5. Test 1 is light vibration with eyes closed, test 2 is light vibration with eyes open, test 3 is heavy vibration with eyes closed and test 4 is heavy vibration with eyes open.

	Correlation between Mx-y				Correlation between Mx-Fy			
	Test 1	Test 2	Test 3	Test 4	Test 1	Test 2	Test 3	Test 4
Subject 1	-0.9478	-0.9267	-0.9605	-0.9267	-0.9681	-0.9457	-0.8875	-0.9255
Subject 2	-0.8808	-0.9158	-0.9195		-0.9619	-0.9599	-0.8993	
Subject 3	-0.8436	-0.8516	-0.9495	-0.9557	-0.9588	-0.9549	-0.9453	-0.9776
Subject 4	-0.8939	-0.9738	-0.9592	-0.9686	-0.8045	-0.9130	-0.8991	-0.9316
Subject 5	-0.9235	-0.9759	-0.9558	-0.9749	-0.9088	-0.9544	-0.8924	-0.9704
Subject 6	-0.8748	-0.9724	-0.8698	-0.8823	-0.9518	-0.9231	-0.9504	-0.9313
Subject 7	-0.8698	-0.8330	-0.9209	-0.9219	-0.9158	-0.9091	-0.9151	-0.8719
Mean	***-0.8906***	***-0.9213***	***-0.9336***	***-0.9407***	***-0.9242***	***-0.9372***	***-0.9127***	***-0.9366***

Table 4.4 Correlation coefficients between Mx-y and Mx-Fy.

In table 4.5 the correlation between y1 (diode 1 placed at the body mass centre) and y2 (diode 2 placed on the thigh) is presented. The correlation between the two points are very large for all subjects in all tests, the two diodes moved almost exactly in the same way, i.e. no flexion took place in the hip.

	Correlation between Fy-y				Correlation between y1-y2			
	Test 1	Test 2	Test 3	Test 4	Test 1	Test 2	Test 3	Test 4
Subject 1	0.8519	0.8092	0.8039	0.7911	0.9887	0.9704	0.9905	0.9508
Subject 2	0.7568	0.8365	0.6918		0.9066	0.8765	0.9924	
Subject 3	0.7330	0.7804	0.8221	0.8949	0.8545	0.9788	0.9066	0.9748
Subject 4	0.5402	0.8499	0.8147	0.8357	0.8806	0.9833	0.9745	0.9825
Subject 5	0.7042	0.8889	0.7834	0.9231	0.9948	0.9820	0.9865	0.9930
Subject 6	0.7238	0.8644	0.6933	0.7803	0.9837	0.9875	0.9684	0.9650
Subject 7	0.6257	0.5843	0.7190	0.6775	0.9751	0.9934	0.9964	0.9927
Median	***0.7051***	***0.8019***	***0.7612***	***0.8223***	***0.9406***	***0.9674***	***0.9736***	***0.9816***

Table 4.5 Correlation coefficients between Fy-y and y1-y2.

The gramians of a 15th order system (light vibrators) and a 20th order system (heavy vibrators) gave model orders for the four tests according to Table 4.6. The model choice criterium was that all states with singular values lesser than a tenth of the largest singular value could be taken out of the model. A model order of n=6 can be used both for test 1 and test 2, a higher order (n=8) must be used for test 3. The correct order for test 4 (heavy vibrators with open eyes) cannot be found since three subjects out of six had an unstable pole distribution. In test 1 one the values of order range from 4 to 9, the mean is 6.7, in test to the range is 3 to 9 with a mean of 6 and in test 3 to 12 with a mean of 8.

Order	Test 1	Test 2	Test 3	Test 4
Subject 1	5	8	3	n.s
Subject 2	9	4	8	
Subject 3	4	5	10	n.s
Subject 4	7	n.s	7	7
Subject 5	6	5	6	6
Subject 6	7	9	9	n.s
Subject 7	9	3	12	10
Mean	***6.71***	***5.67***	***7.86***	***7.67***

Table 4.6 Estimated model order of the four tests.

The low amplitude vibration tests were analysed with a system order of n=6 for all subjects. In test 1 the slower system dynamics is captured by all subjects, but there are large errors in gain and faster dynamics, especially in gain, which is to low for all subjects. The simulations of test 2 gave a very poor result, only the results of subject 3 of the seven subjects were acceptable (i.e. on par with test 1), all the other simulations are very bad.

Test 3 was analysed with a model order of n=8. The deterministic simulation and cross validation gave acceptable results for subject 1, 2 and 7, although the gain (once more) was to low. For subject 3 and 4 the deterministic simulation gave good results, with acceptable gain and good dynamics. The results of the cross validation for these subjects were also good, although the gain was a bit low. Both the deterministic simulation and cross validation were not acceptable for subject 4 and 5, there were large errors in gain and dynamics.
The fourth test gave similar results as the second, only one subject was acceptable identified and all the other were not. The algorithm gives good simulations for the closed eyes tests, but cannot successfully identify the open eyes tests. The results of test 1 for subject 1 is shown in Figure 4.20 all other results are found in Appendix C.

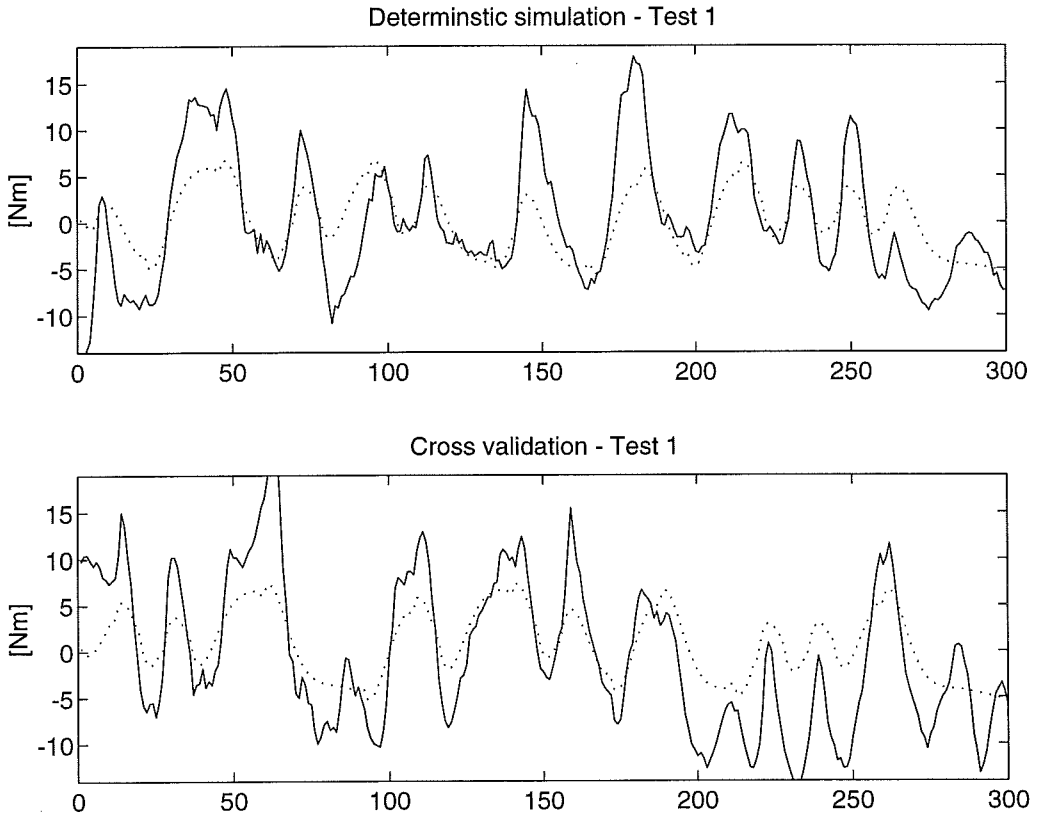

Figure 4.20 Deterministic simulation and cross validation of Mx for subject 1, light vibrations and eyes closed. Dotted line - simulated output, solid line - measured output.

The pole distribution changes during the tests, three different identification periods were examined. In test 1 the imaginary poles of subject 1, 2, 4, 6 and 7 move towards the axis, the pole movements of subject 3 are quite diffuse and the poles of subject 5 move very little. During the whole measurement period every subject exhibits an integrative pole at z=1. In test 2 no pattern in the pole movements can be established except for the integrative pole, which all subjects show (the integrative poles of test 2 are all very close to z=1, more than in test 1). The poles of subject 1 do not move in this test. In test 3 we also have poles at z=1, the other poles are more evenly distributed than for the other test and as for test 2 no pattern of the pole movements is found. The last test once again show that all subjects have the integrative poles, but in this test all subjects also just marginally alter their pole distribution. In Figure 4.21 subject 7 is shown as an example of the pole shift, the pole distributions of the other subjects are found in Appendix C.

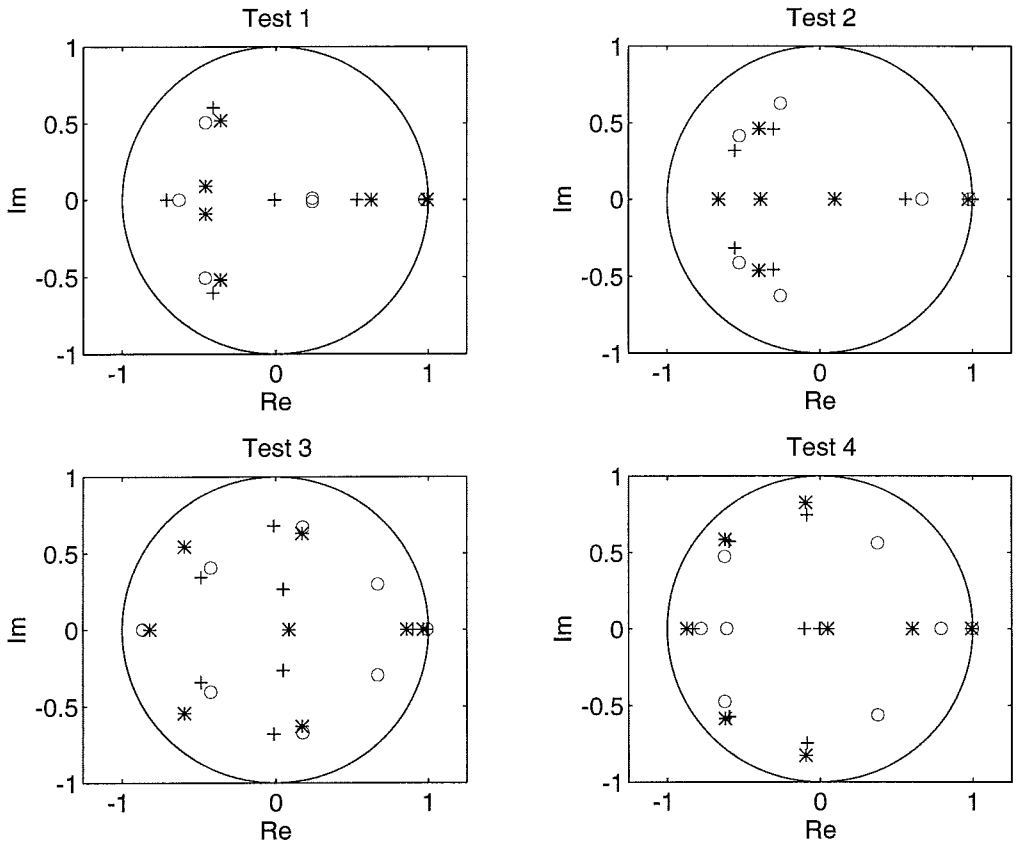

Figure 4.21 Pole shifts of subject seven for all four tests. o - poles of early identifying period, + - poles of middle identifying period, * - poles of late identifying period.

A very high model order, n=100, was tested to find out if the errors in gain could be corrected. The very high order gave a somewhat better performance in both the simulations (i.e., deterministic simulation and cross validation), but the improvement was not that great in comparison to the model order of n=6, and there was almost no differences between an order of 25 or of 100. See Figure 4.22.

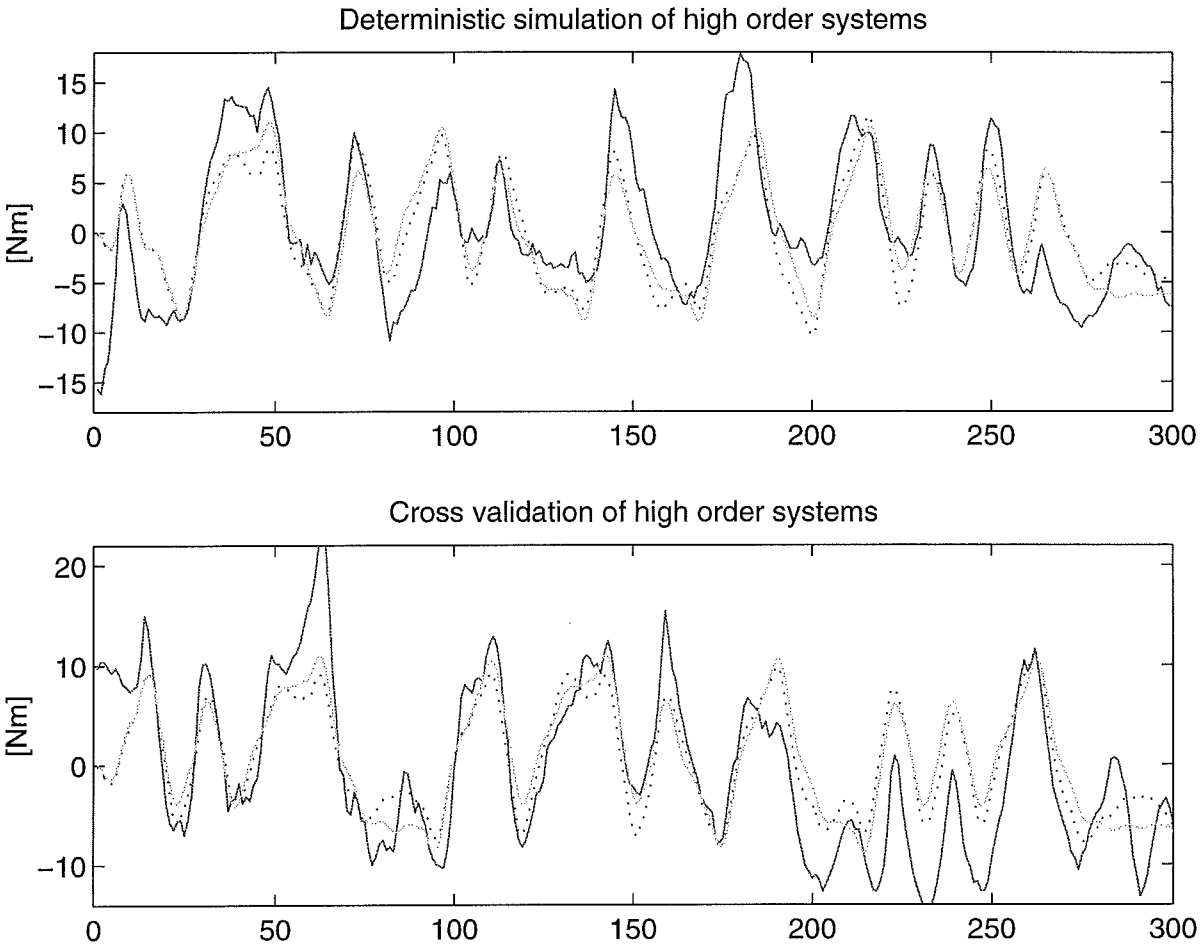

Figure 4.22 Simulation of a very high system orders of n=100 and n=25. Notice the very small difference between the two orders. Dotted line - simulated 100th order Mx output, solid weak line - simulated 25th order Mx output, solid line - measured Mx output.

4.4 Stochastic realisation of residuals

The residuals do not pass the statistical tests and there are difficulties in finding the correct model order. The histograms of output residuals e(k) and residuals w(k) for a system order of n=6 is shown in Figure 4.22. As can be seen most of the residuals are evenly spread around zero and seem to fit rather well to a normal distribution. The spectra of the three output residuals, however, are not that white. The spectra of the two force platform outputs both have peaks around 4.5 7.5 and 9 Hz. The spectrum of the residual in Y exhibit a breakpoint at 5 Hz, lower frequencies show more excitation than higher, this output do also exhibit a peak around 4.5 Hz. The common peaks might be related to the stimulus, which has got a peak around 4.8 Hz. And the low pass charactistics of the Y output might stem from the selspot equipment.

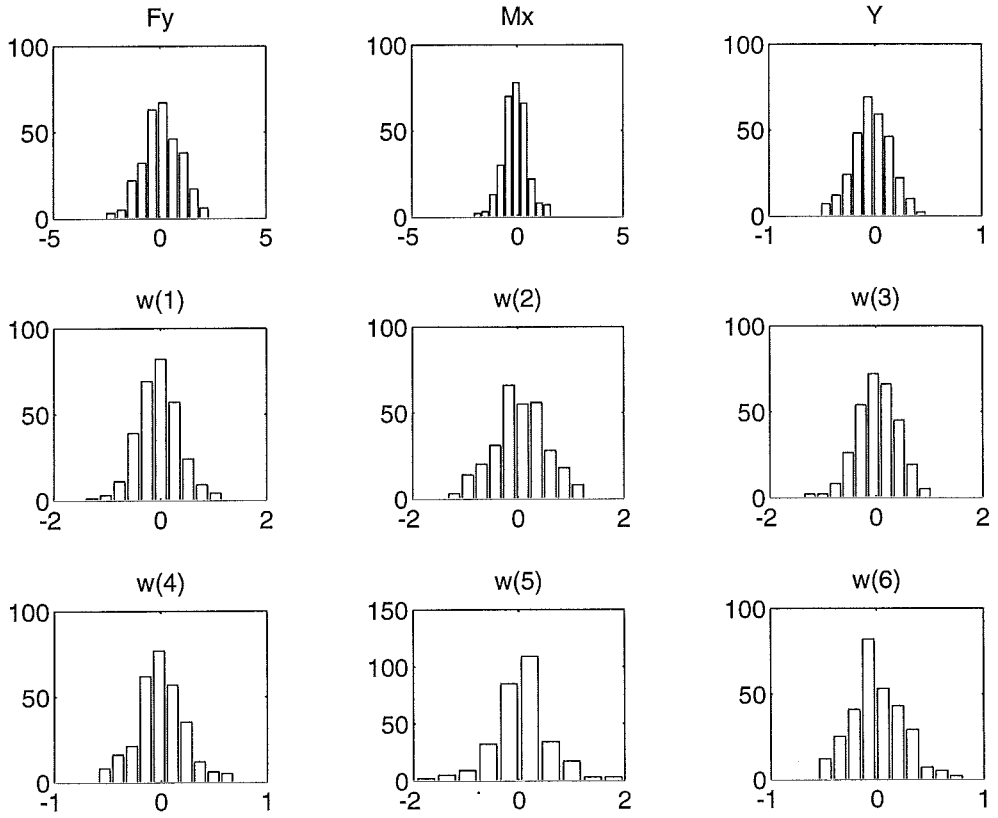

Figure 4.22 Histograms of the residuals of a six-order model.

Each residual sequence was tested in an ARMA model, and validated with autocorrelation test. For a system order of n=6 the output residuals could be described as a three to six order model and the other residuals with a five to eight. When the original system order was doubled to n=12 the noise model order of the ARMA approach dropped to two or three for the output residuals, but for the other residuals there was no such drop. The e(k) residuals had all smaller test values in the autocorrelation test (still they did not pass the test) for the high system order and the w(k) residuals had higher test values for the higher order. Even for a system order of 25 (compare Figure 4.21) none of the w(k) residuals did pass the test. In Table 4.7 the order of the A and C polynomials are shown for each output residual respectively.

Residual	A (n=6)	C (n=6)	A (n=12)	C (n=12)
Fy	6	6	2	2
Mx	5	5	3	2
Y	3	3	3	2

Table 4.7 Order of the A and C polynomials in Arma noise model. Output residuals.

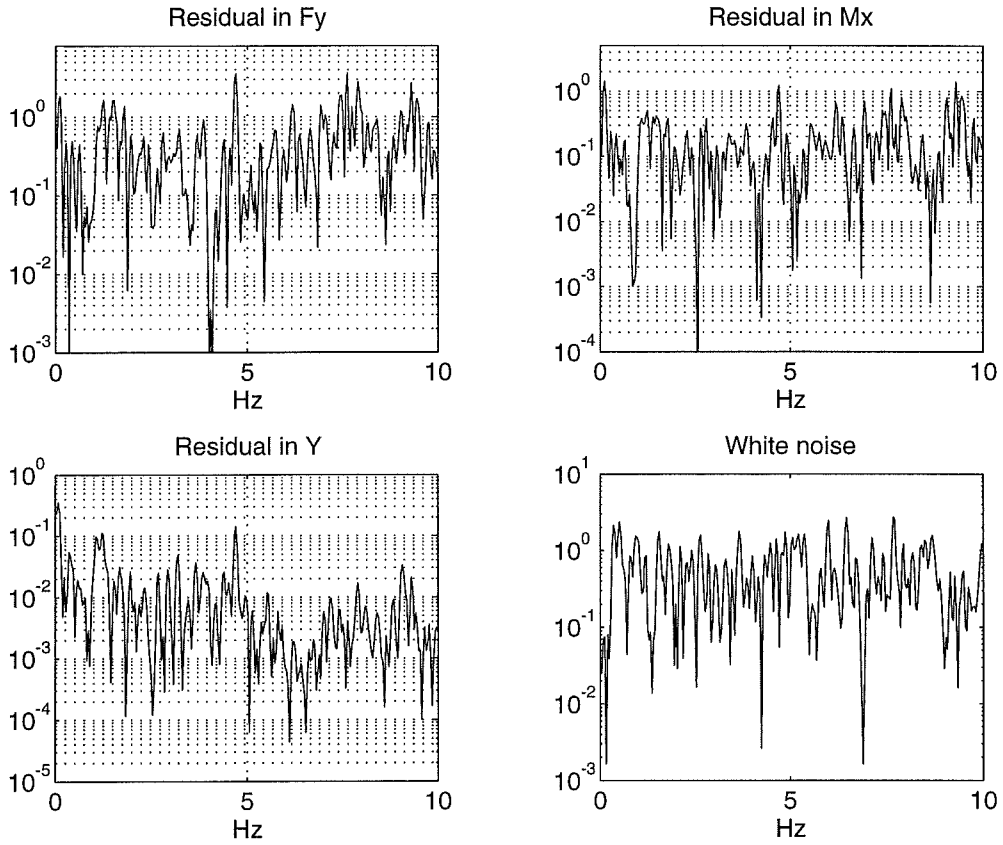

Figure 4.23 Spectra of the three output residuals and of white-noise.

The output residuals in Fy and Mx can be considered white for a high model order (for example did the residuals of subject 1 in test 1 indicate a model order of 25) and the Y residual can be modeled with a noise model of order 2 or 3. The w(k) residuals must be modeled with an higher noise model order somewhere between 5 and 9, this model should be in a balanced state space representation using the algorithm for stochastic realisation found in [Johansson 95]. In Figure 4.24 the poles and zeros for a second order ARMA noise model for residual in Y together with a six order ARMA model for w(1) are depicted. The residual in Y have two just slightly damped pole-zero pairs close to the unit circle, which leads to a very oscillating behaviour (note although the poles and zeros lie close to each other they cannot be cancelled out, if the model order test shall be passed). The pole-sero distribution of w(1) have one integral pole and damped pole-zero pairs, this configuration results in a very large overshoot before the system is damped out.

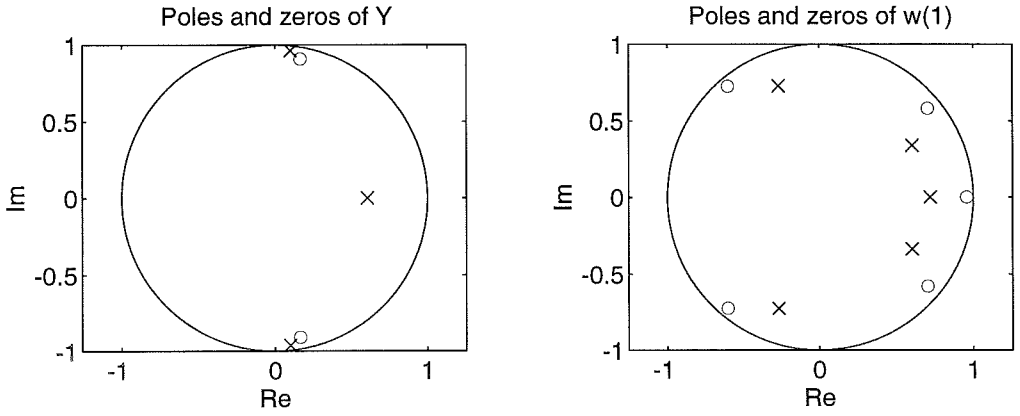

Figure 4.24 Poles and zeros of two residuals.

5 Discussion

The relevant outputs in the identification are the three sagittal outputs, all the other are either not affected by the stimulus (Mz and z), to disturbed (Fz) or non linear (Fx, My and x). The nonlinearity of these outputs can be described as random. The person can fall to either side, things that could affect the direction of the sway are, vibrator placement (i.e., asymmetric stimulation), the subject's former movements, placement of the feet etc. The coherence of Mx; Fy and y and the input was acceptable, the coherence was tested between each output and the input as for a SISO-system. A multi variable coherence function approach, where these three outputs were tested together against the PRBS-signal, were also examined but gave not a higher coherence.

There are a strong correlation between the sagittal torque and the movement of the body mass centre, which indicates that the inverted pendulum is a sufficient model both for high and low amplitude stimulation. A fact confirmed by the large correlation in the movements of the two diodes, which means that no flexion takes place in the hip. But there are also very large shear forces, which should according to the theory [Johansson and Magnusson] only appear when the subject are about to overcome a large disturbance, but for all subjects and in all tests shear forces do appear. It must be remembered that although no flexion takes place in the hip, still the subjects might bend their knees. A new experimental set-up, that allow measurements of the position of all body segments, should then be used (see Appendix D). The large correlation between shear force and torque shows, that the shear force is directed in the opposite direction as the torque and large shear forces correspond to large moments, i.e., the shear force is largest at the end of a "sway" cycle. Notice that the shear force is always present when the subject sways, even if just a small perturbation is induced as in the case of low amplitude stimulation. It is also somewhat surprising that the correlation is as good or even better with heavy vibrators than with light, the pilot tests gave another result. Of course, the subjects of the pilot tests might be non-characteristic subjects, but the result might also depend on the test order. The subjects become accustomed to the stimulation during the first test, and have already found an optimal control strategy when the heavy vibrators are used.
There are large differences between the subjects in each test in how well the algorithm can simulate and predict the outputs. Test 1 and 3 (the test with closed eyes) give good results for almost all subjects. Only those subjects that respond mildly to the stimuli cannot be simulated. In test 1, for instance, subject 2 and 7 exhibit the largest discrepancies between real and simulated output, these two had both a model order of n=9 in the balanced realisation test and a model order of n=6 is not enough to capture their sway dynamics. These two also have the smallest sway amplitude (approximately 5 Nm) but they have a much more high frequent sway (especially subject 7), they seem to use very small but fast changes to maintain their posture. In this test the simulation of subject 5 shows a time delay (the simulated output lies ahead of the real output), this is rather strange since subject 5 was the only one that had a model order of n=6 in the balanced realisation test. The results of the third test are almost better than for the light vibrator test, once more a discrepancy between the main study and the pilot test.
The poor simulations of test 2 and 4 (open eyes test) are due to a much smaller and non linear response to the stimulus by the subjects when they can use the sight to guide them (the result was expected the coherence between the Mx-torque and the stimulus has been found to be weaker with open eyes [Johansson et al 88]).
The pole distributions of test 1 show a tendency that the subjects adopted a more stable control strategy, this could not be said for the other tests, but there is a pole shift in test 2 and 3, and thus an adaptation to the stimulus (especially in test 3). But still the cross validations yield good results, the system is therefore just slightly time variant. This is not true for test 4, where the poles hardly move at all. Once again this might be explained by the test order. The subjects' adaptation to the stimuli takes place mainly during their first contact with the induced disturbances, even though this is a relatively small disturbance. Still, the higher model order of the heavy vibrator tests seem to force the subjects to adopt a more complex control strategy. The poles on the real negative axis might be explained by aliasing, an oscillating high frequency disturbance (most likely a 50 Hz net disturbance) is folded into the real measurements. An analogue low-pass filter should be used to exclude these errors.
Notice the small differences between the fifteen-order system and the six-order system in the simulations, the algorithm is very robust to overparametrization.
It is very hard to find an optimal model order, since there does not appear to be any clear criteria of optimisation. The statistical residual tests behave very strange without any clear pattern and the balanced realisation did not give one clear model order for each test, the correct order varies probably from subject to subject. The algorithm's noise model of the w(k) residuals must be further researched. A possible method to locate the correct model order is to find the model order, where the residuals in torque and shear force are white and then simulate systems with a somewhat higher and lower order. The one that gives best simulation is to be chosen. Since the model order, where the force residuals become white is high (around 25-30) this method is time costly.
The different tested values of the block row number r show that this value is of a crucial importance to the algorithm, the optimal r-value is either the minimum r=n or a larger value of at least r=n+6. A larger value means that more data points is included in the analysis and that the Hankel matrix becomes less rectangular (if s is not altered). Why r-values between n and n+6 induce a false time delay and in general give worse simulation results remains to be examined.

6 Conclusions

Relevant outputs for the identification of calf stimulation studies are the sagittal torque (Mx), the shear force in the sagittal direction (Fy) and the sagittal coordinate of the body mass centre (y). All these outputs are for both cases of stimulation (heavy and light vibrators) and test made with eyes open and eyes closed correlated to each other. The correlation is largest between Mx and Fy, the shear force is present during the whole sway cycle. There are no twisting movement or up and down movement. The responses in lateral torque (My), lateral coordinate (x) and shear force in the lateral direction to the stimulus are non linear. The identified systems of all four tests have an integral part and there is a tendency to a alteration to a more stable control strategy in test 1. The model order is six for the tests made with low amplitude stimulation and eight for the tests made with high amplitude stimulation.
The subspace algorithm is adequate to identify the human postural control system in the tests made with closed eyes. The model order algorithm is prone to noise and an optimal model order is hard to find in both the heavy and light vibrator case. The statistical tests of the residuals cannot be used, in order to find the model order. The best method is instead a balanced model reduction or simulation, but a new noise model, especially for the w(k) residuals, is needed. Larger block row number, r, than the minimal (r=n) causes errors in the identification. The algorithm is robust to overparametrization.

Further fields for studies are
- r-value
- residual model
- model order algorithm
- model order optimisation

References

[Dietz 92] V. Dietz. Human Neuronal Control of Automatic Functional Movements: Interaction Between Central Programs and Afferent Input. *Physiological Reviews,* 72:33:68, 1992.

[Johansson et al 88] R. Johansson, M. Magnusson and M. Åkesson. Identification of Human Postural Dynamics. *IEEE Transactions Biomedical Engineering*, 35:858-869, 1988.

[Johansson and Magnusson 91] R. Johansson and M. Magnusson. Human Postural Dynamics. *CRC Critical Reviews in Biomedical Engineering,* 18:413-437, 1991.

[Johansson 93] R. Johansson. System Modeling and Identification. *Prentice Hall Information and System Sciencies Series,* 1993.

[Johansson 95] R. Johansson. State-space Methods. *Draft to chapter 16 in System Modeling and Identification,* 1995.

[Moonen et al 89] M. Moonen, B. de Moor, L. Vandenberghe and J. Vandewalle. On- and off-line identification of linear state-space models. *International Journal of Control,* 49:219-232, 1989.

[Pyykkö et al 83] I. Pyykkö, G. Å. Hansson, l. Schalén, N. G. Henriksson, C. Wennmo, M. Magnusson. Vibration Induced Body Sway. *Computers in neuorotological diagnosis,* 139-155, 1983.

[Verhaegen and Dewilde 92] M. Verhaegen and P. Dewilde Subspace Identification Part 1. The output-error state-space model identification class of algorithms. *International Journal of Control,* 56:1187-1210, 1992.

Appendix A - Selspot equipment

The Selspot equipment consists of two CCD -cameras, a control unit and two Light Emitting Diodes. The coordinates of a diode is interpreted as two voltages, which are proportional to the vertical and horizontal distances between the diode and the camera's line of convergence. Two cameras are used to determine the coordinates of a Cartesian coordinate system, x y and z.

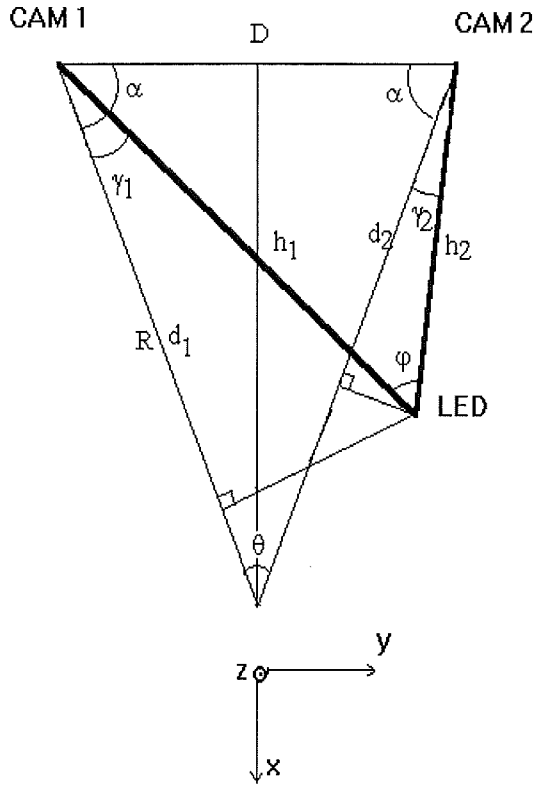

Figure. A.1 Configuration of the Selspot equipment, together with the coordinate system of the force platform.

Camera i (i=1,2) gives the horizontal voltage U_{xi} and the vertical voltage U_{zi}. Trigonometry with notations according to figure A.1 gives:

$$d_1 = h_1 \cdot \cos\gamma_1$$
$$d_2 = h_2 \cdot \cos\gamma_2$$
$$h_1 = D \cdot \frac{\sin(\alpha + \gamma_2)}{\sin\varphi}$$
$$h_2 = D \cdot \frac{\sin(\alpha - \gamma_1)}{\sin\varphi}$$

with $\varphi = \pi - (2\alpha - \gamma_1 + \gamma_2) = \theta + \gamma_1 - \gamma_2$ and the sine theorem we have,

$$d_1 = D \cdot \frac{\sin(\frac{\pi}{2} - \frac{\theta}{2} + \gamma_2)}{\sin(\theta + \gamma_1 - \gamma_2)} \cdot \cos\gamma_1$$
$$d_2 = D \cdot \frac{\sin(\frac{\pi}{2} - \frac{\theta}{2} - \gamma_1)}{\sin(\theta + \gamma_1 - \gamma_2)} \cdot \cos\gamma_2$$

In order to find the dependence between the distance lens-diode plane and the voltage, the difference in voltage between two points 20.0 cm apart were measured for six distances. Three pair of points were examined for every distance, thus a scale factor (cm/V) was calculated. The scale factors were plotted against the distances and the linear dependence between coordinate, voltage and distance was computed. These were found to be:

Camera 1

$$x_1 = U_{x1} \cdot (0.0401 \cdot d_1 + 0.3399)$$
$$y_1 = R - d_1$$
$$z_1 = U_{z1} \cdot (0.0399 \cdot d_1 + 0.5614)$$

Camera 2

$$x_2 = U_{x2} \cdot (0.0405 \cdot d_2 + 0.2637)$$
$$y_2 = R - d_2$$
$$z_2 = U_{z2} \cdot (0.0423 \cdot d_2 + 0.2086)$$

As every voltage in the horizontal plane corresponds to an unique angle, γ_i can be determined as

$$\gamma_1 = \arctan(0.0401 \cdot U_{x1})$$
$$\gamma_2 = \arctan(0.0405 \cdot U_{x2})$$

The coordinates are then transformed into the coordinate system of the force platform:

$$x = (-x_1 - x_2) \cdot \cos\tfrac{\theta}{2} + (-y_1 + y_2) \cdot \sin\tfrac{\theta}{2}) / 2$$
$$y = (x_1 - x_2) \cdot \sin\tfrac{\theta}{2} - (y_1 + y_2) \cdot \cos\tfrac{\theta}{2}) / 2$$
$$z = (z_1 + z_2) / 2$$

In the measurements the platform was placed 120 cm from the cameras and the following values of D, R, α and θ were used:

$$D = 63\,cm$$
$$\theta = \tfrac{2}{15}\pi$$
$$\alpha = \tfrac{11}{15}\pi = \pi - 2 \cdot \alpha$$
$$R = 151{,}5\,cm = D / (2 \sin\tfrac{\theta}{2})$$

The calibration procedure for each camera can be summarised:

1.Two LED:s were placed 20.0 cm apart, both placed left of the camera's zero line (both LED:s gave a negative voltage). A scale factor (cm/V) was computed according to: $\frac{20}{\left|(V_{LED2} - V_{LED1})\right|}$, where V_{LEDi} is the voltage shown by LED i.

2.The procedure was repeated with one LED placed to the right of the camera's horizontal zero line and one to the left. The LED:s were placed on the vertical zero line. A new scale factor was computed.

3. The procedure was repeated with both LED:s placed right of the camera's zero line. A new scale factor was computed.

4. The mean value of the three scale factors were used a new scale factor for the distance resulting.

5. The scale factors for the distances 100 cm, 110 cm, 120 cm, 130 cm, 140 cm and 150 cm were plotted against the distance and the linear regression were computed.

6. The above steps were repeated for the vertical voltages.

The precision of the measurements are restricted by the following facts:

-The AD-converter in the camera is a10 bit-converter, which means that 1024 voltage values are available to represent the analogue voltage (coordinate)
-The error due to noise in the AD-converter is one bit
-The adjustment of the camera placement, especially the setting of the correct angle α
-Nonlinearities in the cameras (especially in the outer ranges, i.e. close to +5V and -5V)

Appendix B - Description of signals

The input signal used is a pseudorandom binary sequence (PRBS), which means that the vibrators are switched on and off without any harmonic pattern. During the stimulation the vibrations is considered to be always on, although the vibrators have a frequency of 60 Hz. The nine outputs measured (the case of one diode) are correlated to each other according to laws of mechanics. The output can be described as follows:

Fx - The shear force directed in the same plane as the lateral sway, i.e. sideboards.
Fy - The shear force directed in the same plane as the sagittal sway, i.e. forwards and backwards.
Fz - The force in the vertical plane, i.e. up and down.

Mx - The torque that induces a sway in the sagittal direction. Notice Mx is the torque around the x-axis.
My - The torque that induces a sway in the lateral direction. Notice My is the torque around the y-axis.
Mz - The torque that induces a twisting sway, i.e. a rotation around the vertical axis. Notice Mz is the torque around the z-axis.

x - The coordinate in the lateral direction.
y - The coordinate in the sagittal direction.
z - The coordinate in the vertical direction.

In Figure B.1 the coordinate system of the platform is depicted.

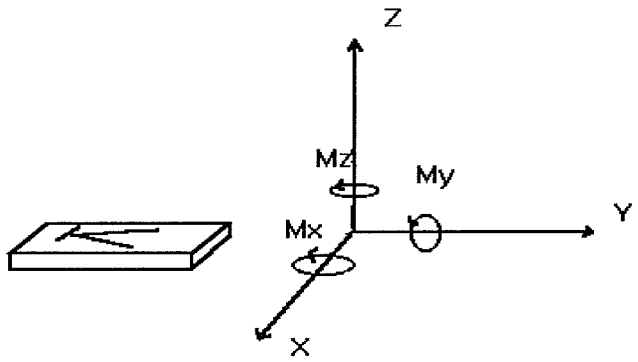

Fig. B.1 Coordinate system of the force platform.

Appendix C - Simulations and pole distribution

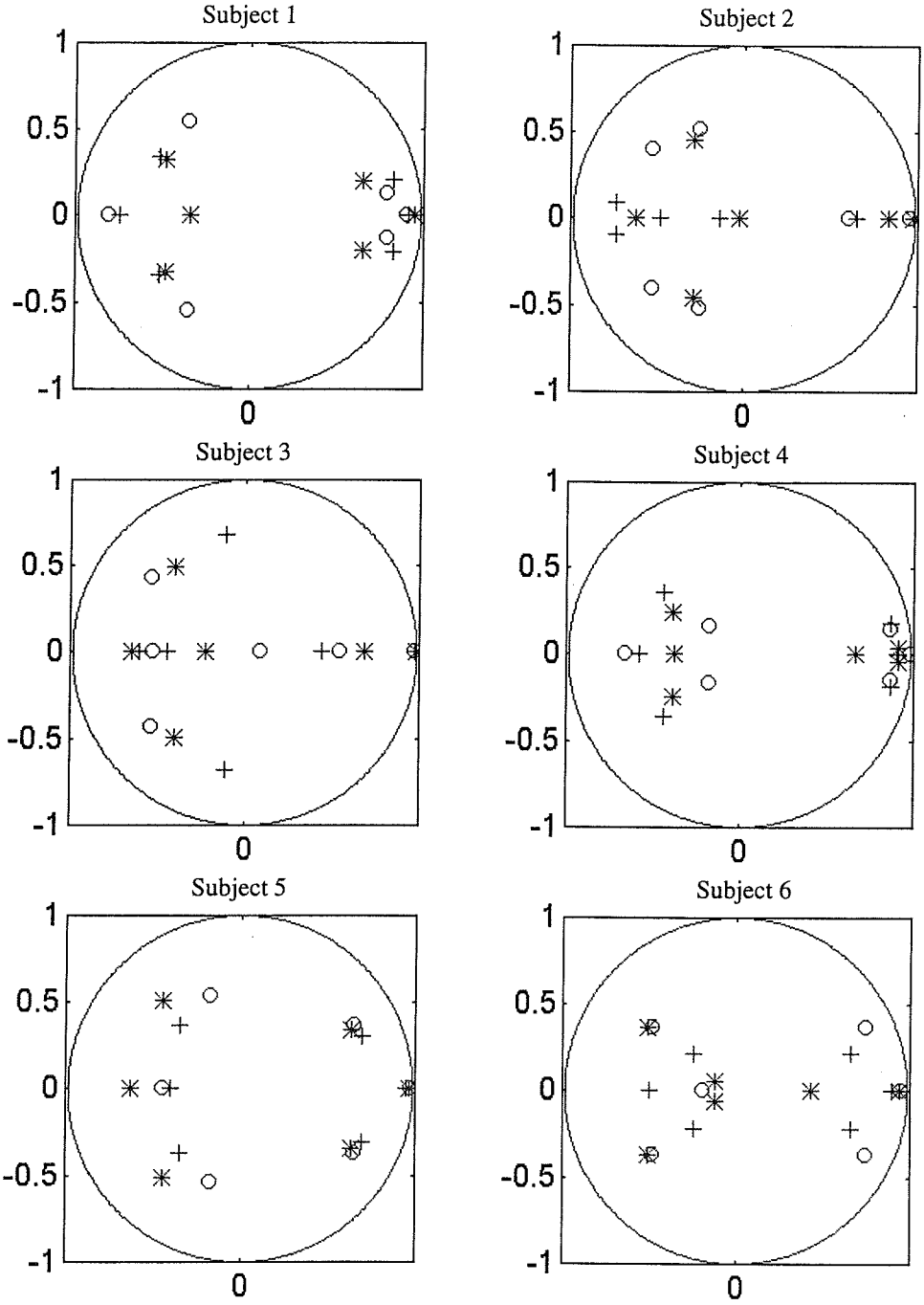

Pole distribution of subject 1 to subject 6 for test 1.
o - early identifying period
+ - middle identifying period
* - late identifying period

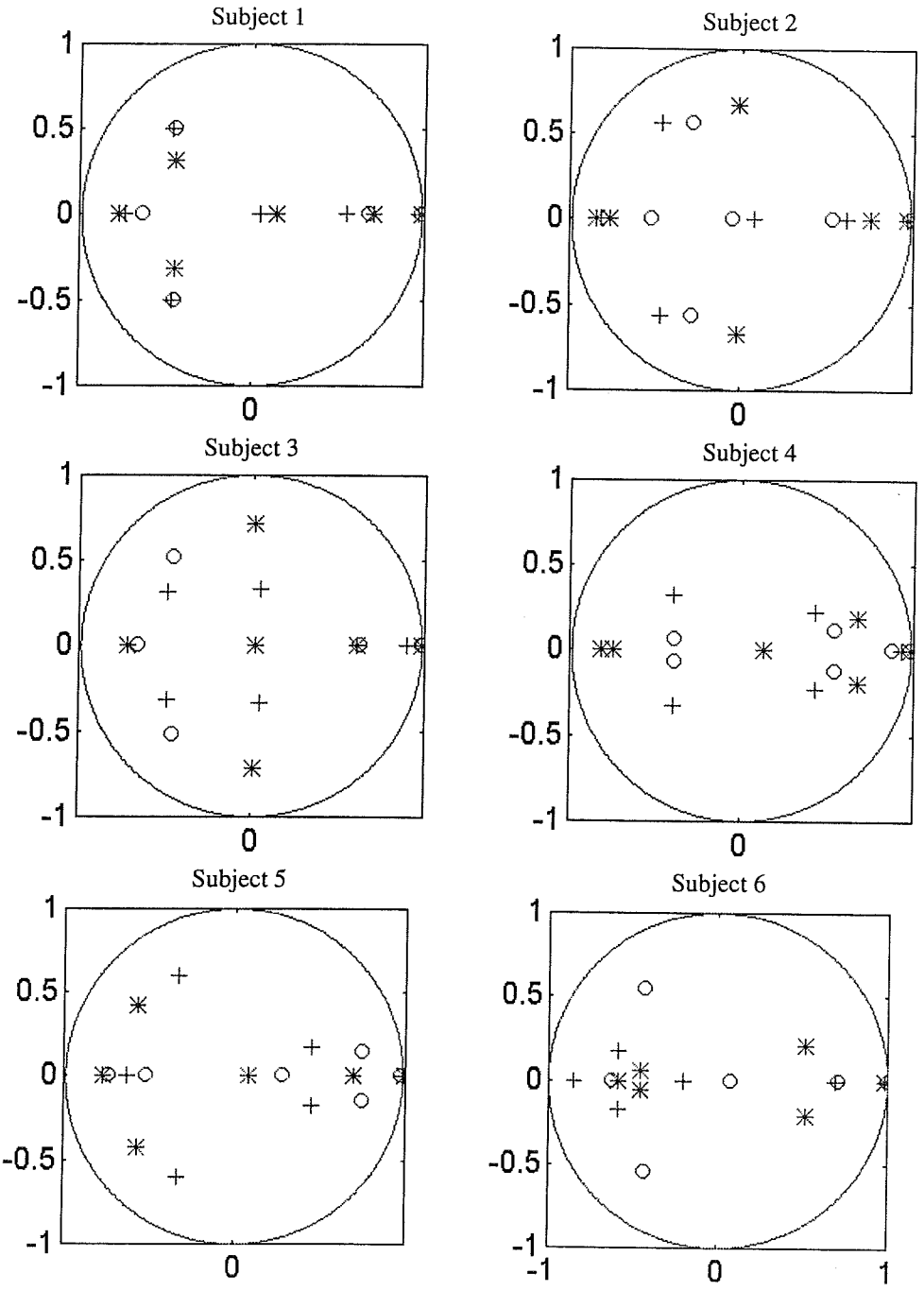

Pole distribution of subject 1 to subject 6 for test 2.
o - early identifying period
+ - middle identifying period
* - late identifying period

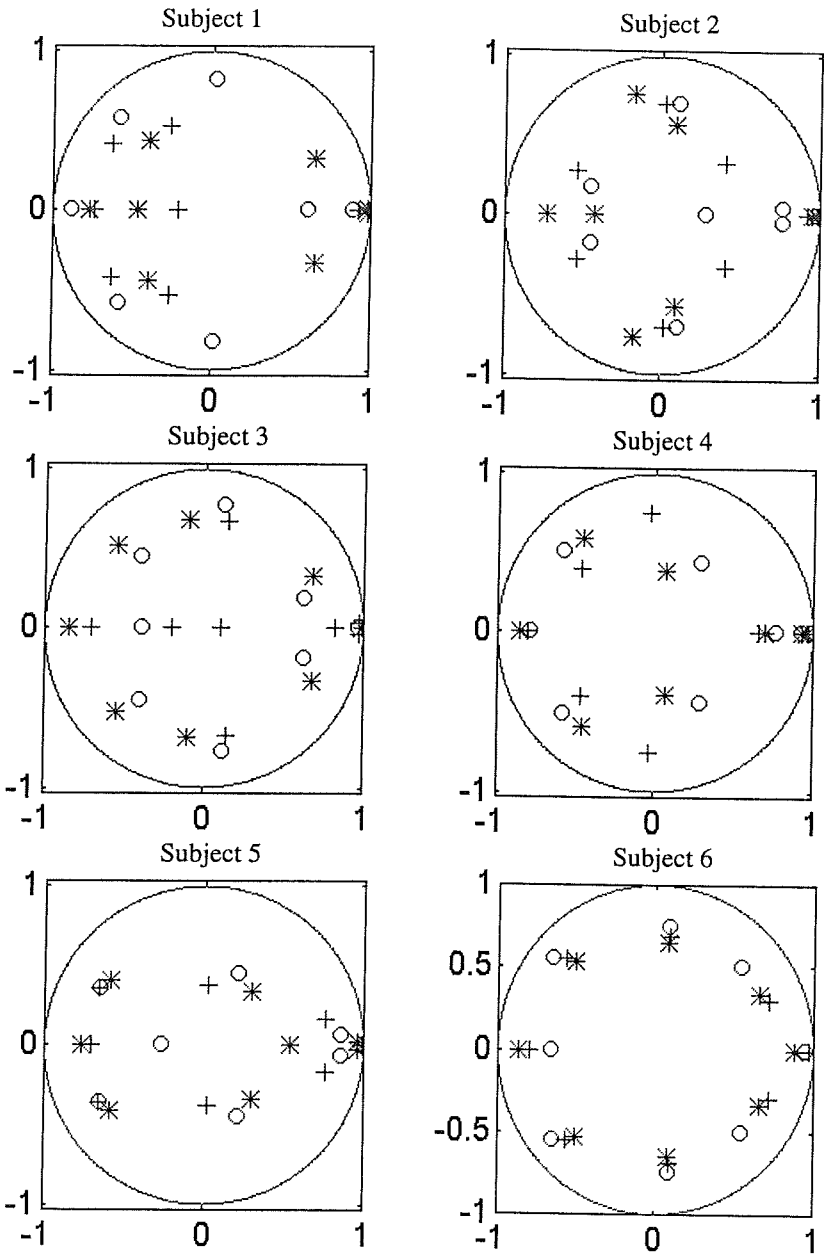

Pole distribution of subject 1 to subject 6 for test 3.
o - early identifying period
+ - middle identifying period
* - late identifying period

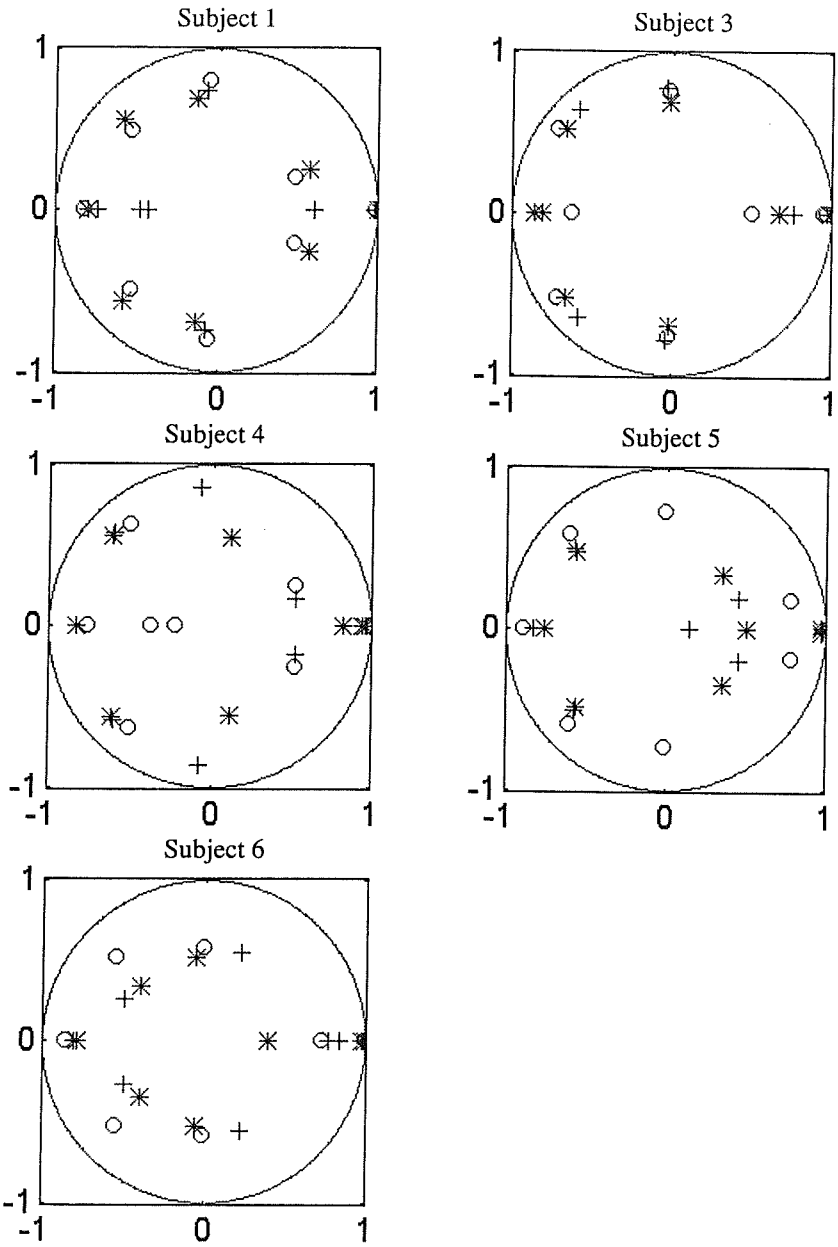

Pole distribution of subject 1, 3, 4, 5 and 6 for test 2.
o - early identifying period
+ - middle identifying period
* - late identifying period

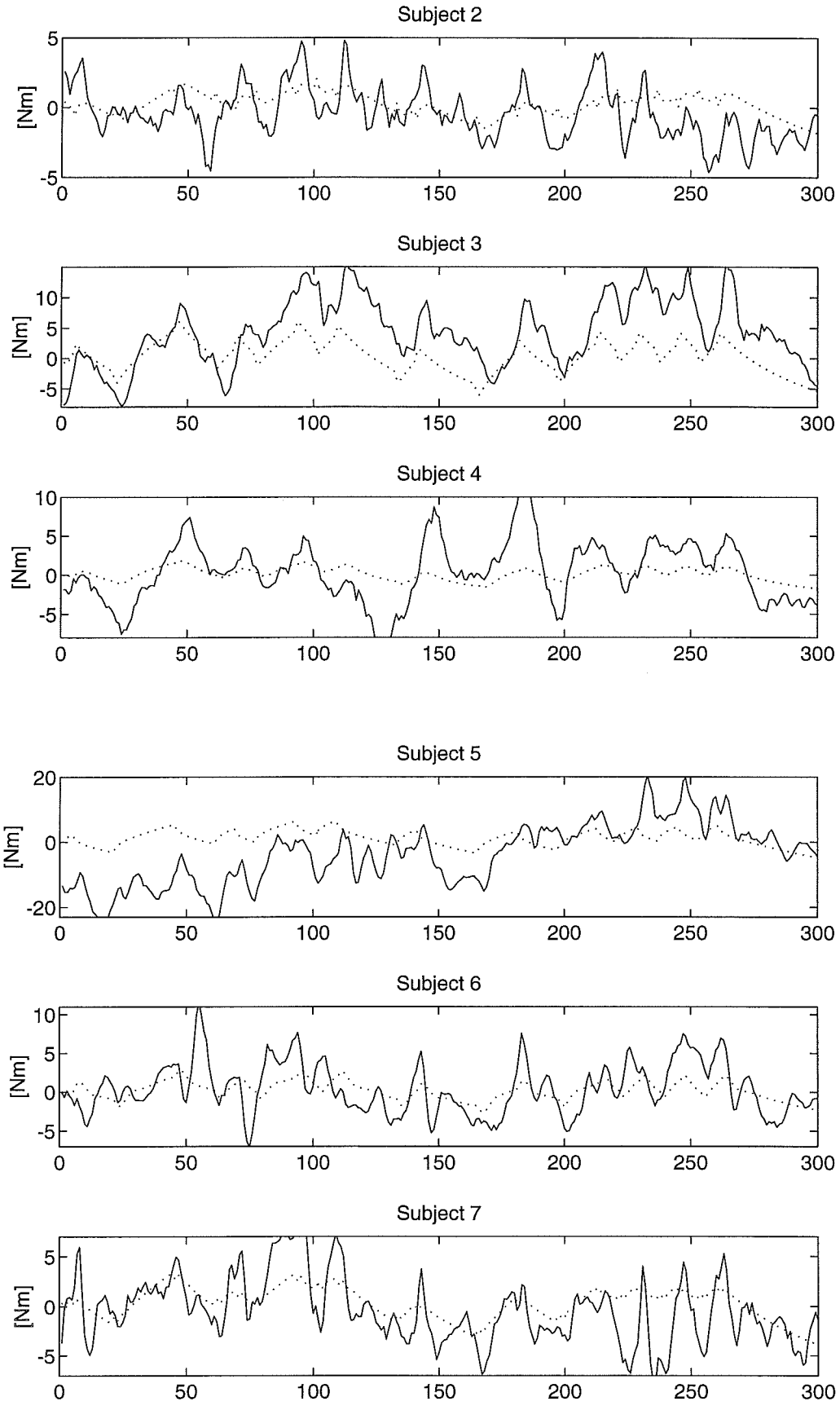

Figure C.1 Deterministic simulation of Mx for Test 1 (Eyes closed, light vibrations)
Dashed line - simulated output; Solid line - measured output.

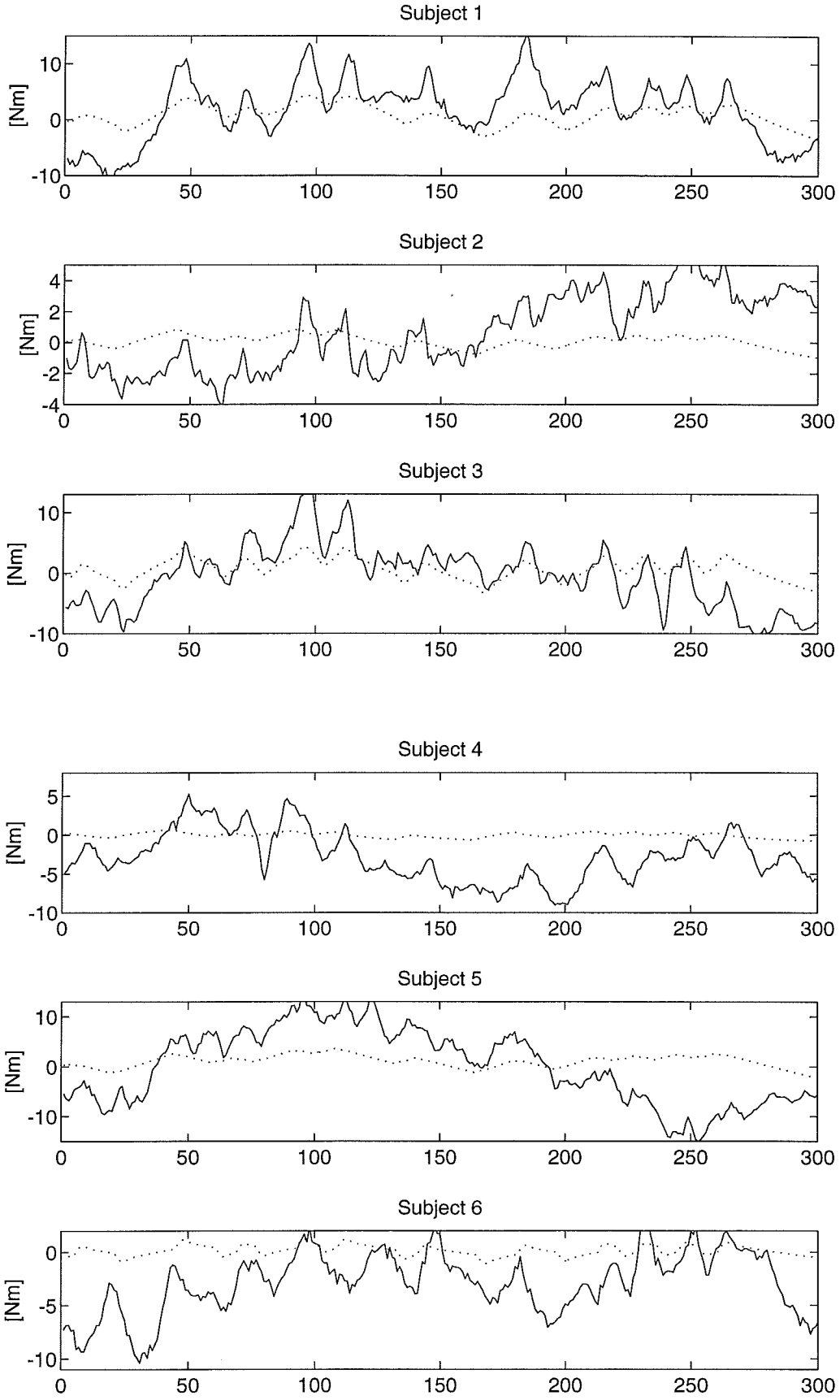

Figure C.2 Deterministic simulation of Mx for Test 2 (Eyes open, light vibrations)
Dashed line - simulated output; Solid line - measured output.

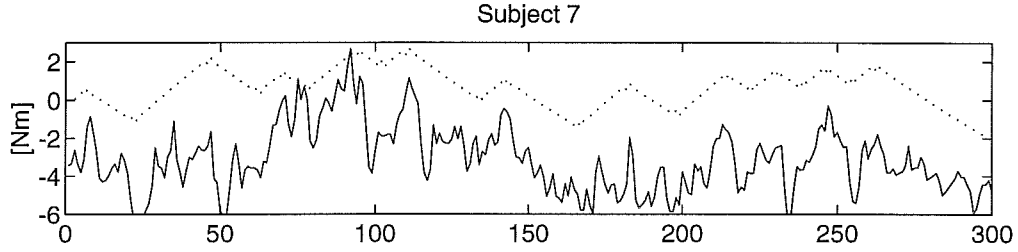

Figure C.3 Deterministic simulation of Mx for Test 2 (Eyes open, light vibrations)
Dashed line - simulated output; Solid line - measured output.

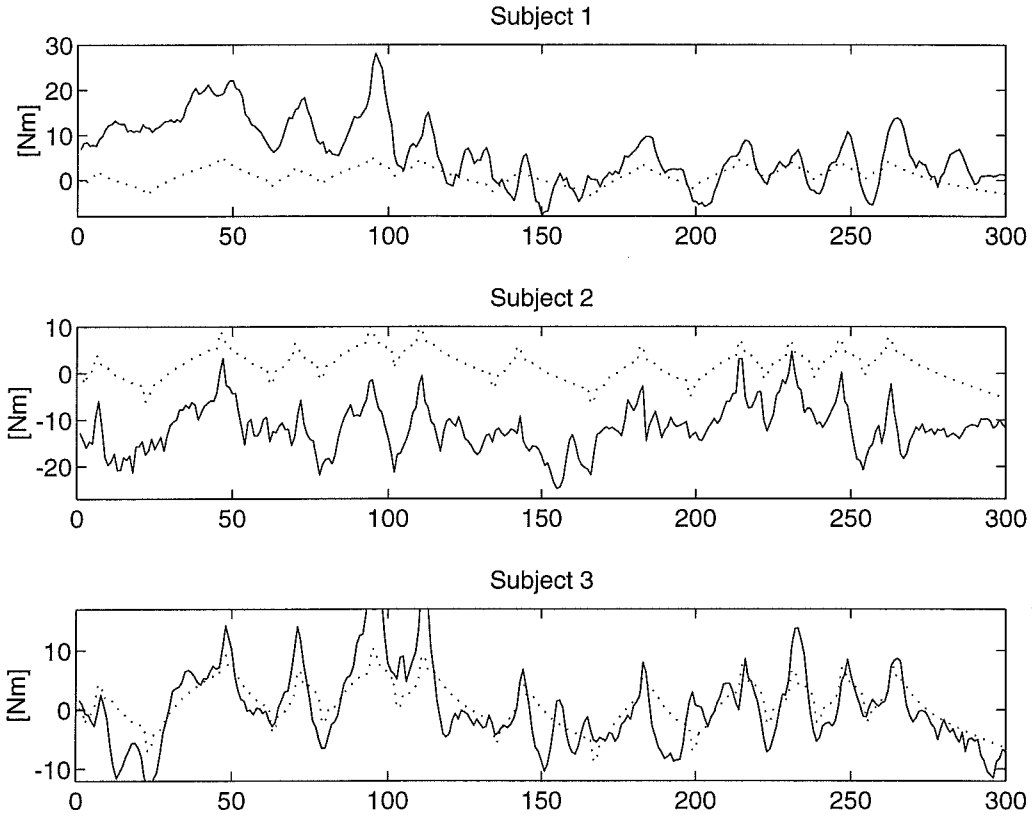

Figure C.4 Deterministic simulation of Mx for Test 3 (Eyes closed, lheavy vibrations)
Dashed line - simulated output; Solid line - measured output.

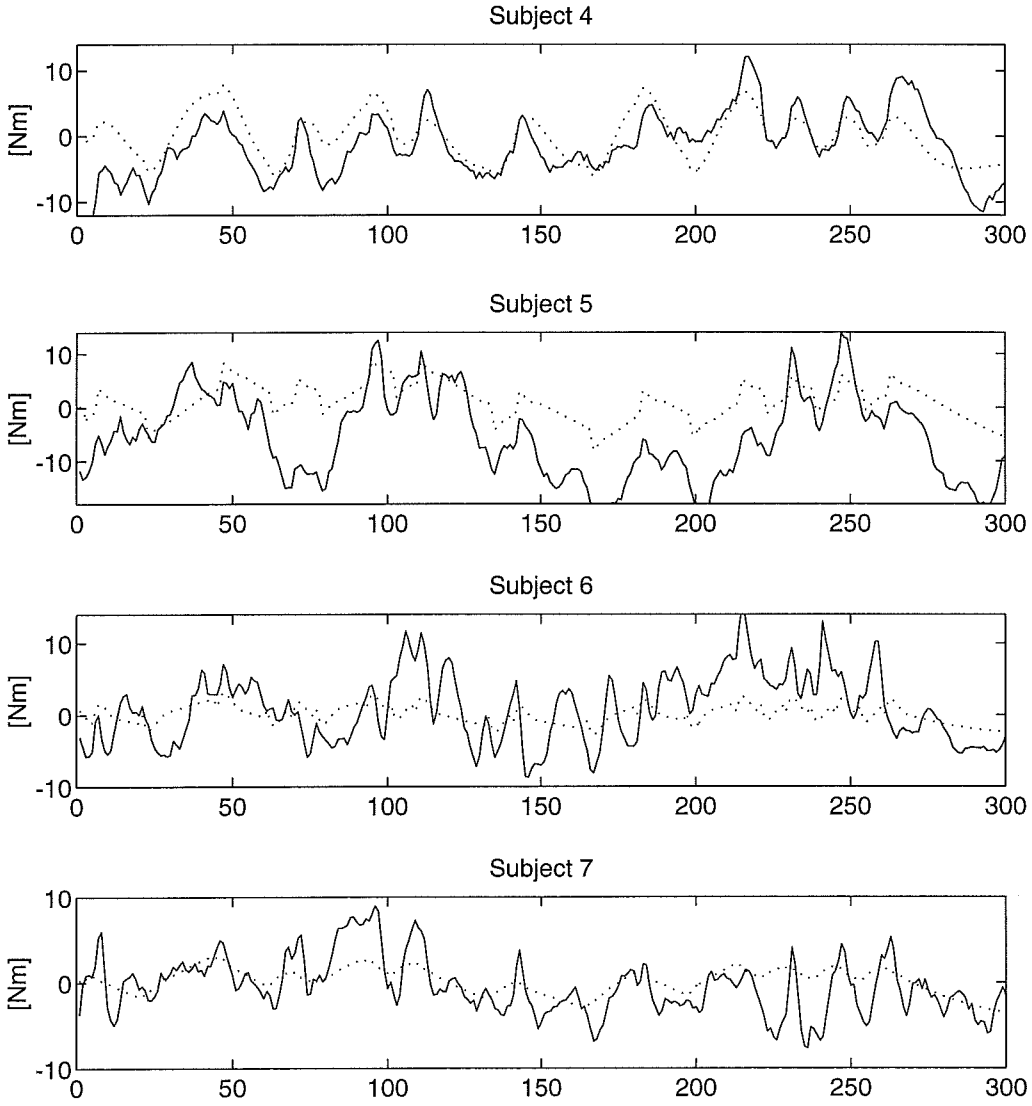

Figure C.5 Deterministic simulation of Mx for Test 3 (Eyes closed, heavy vibrations)
Dashed line - simulated output; Solid line - measured output.

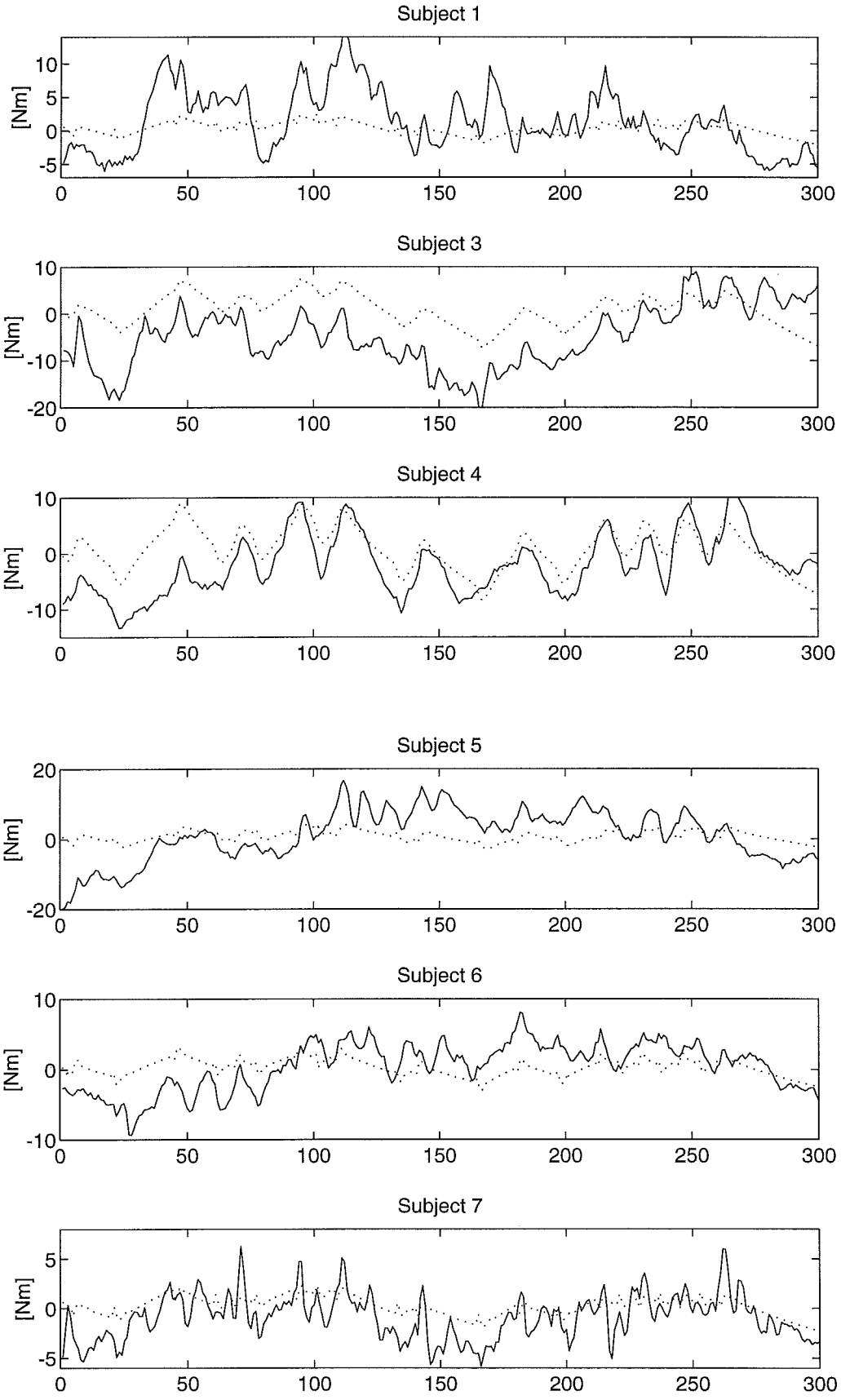

Figure C.6 Deterministic simulation of Mx for Test 4 (Eyes open, heavy vibrations)
Dashed line - simulated output; Solid line - measured output.

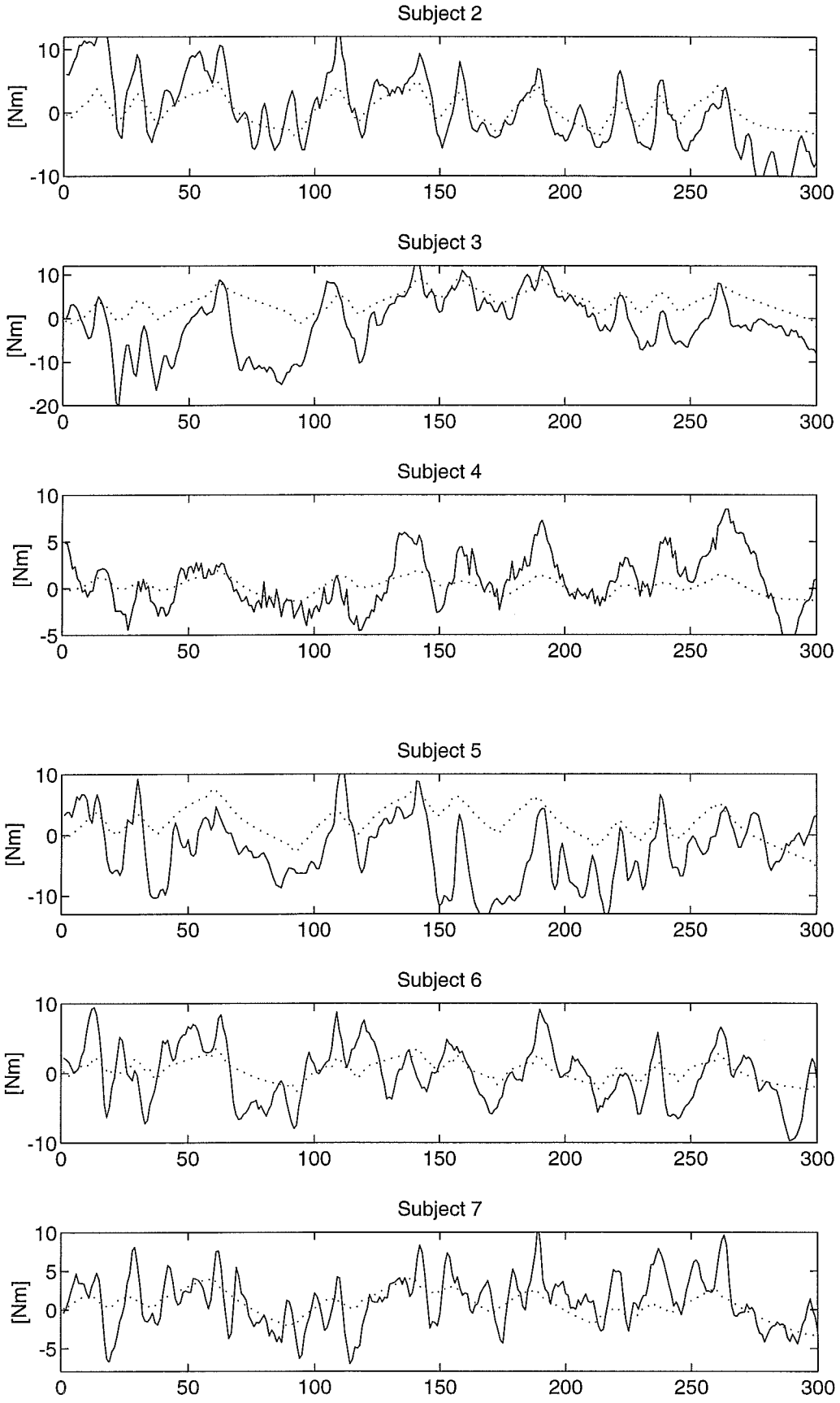

Figure C.7 Cross validation of Mx for Test 1 (Eyes open, heavy vibrations)
Dashed line - simulated output; Solid line - measured output.

Appendix D - Suggestion for further works

A measurement set-up that could prove useful in order to get a better characterisation of calf stimulation is a use of another measuring tool - the EMG-equipment . Together with measurement of forces, torques and coordinates the recordings of the inner muscle activity can give the outputs that are missed in the set-up used in this paper.
The relevant torques/forces are Mx and Fy, the cameras should be placed at different height each with two LED:s. The lower camera should measure the position of a diode placed on the ankle and the position of a diode placed on the lower part of the leg. The other camera should measure the movements of the thigh and the torso, so that different body segment motion could be measured.The EMG-equpment should measure the muscle activity in the calf muscles.
The advantages with such a Selspot set-up is that a very careful calibration at just a small distance interval can be made (for instance by measuring twenty different positions for every distance) and that the problem with the setting of a correct angle is avoided. The camera is calibrated were it is used. The major disadvantage (in fact the only one) is that no lateral movements of the body segments can be measured.
A multi-stimulus multi response measurement with yet another input, galvanic stimulation, combined with the calf stimulation should also be examined.

Appendix E - Matlab macros

sspace.m

```
%sspace
%SUBSPACE IDENTIFICATION
%The main program for the identification of
%postural human control
%Jonas Ekblad 951101
%p number of outputs
%m number of inputs
%n system order
%r block row number
%timeshift timeshift between hankel matrices
%s number of data points

%Initiation of variables
clear;
p=4;
m=1;
n=25;
r=n;
timeshift=r;
s=300;

%loading of file
infile=input('File name ?  ','s');
disp(' ');
disp('The file is loaded');
eval(['load',' ',infile]);
disp(' ');
nfile=infile(1:length(infile)-4);
eval(['z=',nfile,';']);
disp('The computation of the system matrices takes
about 3 minutes');

%Creation of output and input
%using functions forcepl and coord
Yraw1=z(:,1:6)';
Yraw2=z(:,8:11);
Yraw3=z(:,12:15);
Yforce=forcepl(Yraw1);
Ycoord1=coord(Yraw2);
Ycoord2=coord(Yraw3);
Yd=[Yforce(2,:);Yforce(4,:);Ycoord1(:,1)';Ycoord2
(:,1)']';
Ud=z(:,7);

%Detrending of data
Ys=dtrend(Yd,1)';
Us=dtrend(Ud)';

%Where in the data sequence to be identified
Y=Ys(:,1050:2000);
U=Us(:,1050:2000);

%The timeshifted matrices are created
[Yh1,Uh1]=hankel1(Y,U,p,m,s,r,0);
[Yh2,Uh2]=hankel1(Y,U,p,m,s,r,timeshift);

%The new state space vector is created
Z1=[Yh1;Uh1];
Z2=[Yh2;Uh2];
Z=[Z1;Z2];

%The svd for the new state space vector is
calculated
[Using,Ssing,Vsing]=svd(Z);

%Calculation of U11, U12, Sigma11
U11=Using(1:((m+p)*r),1:(2*m*r+n));
U12=Using(1:((m+p)*r),(2*m*r+n+1):(2*(m+p)*r);
Sigma11=Ssing(1:(2*m*r+n),1:(2*m*r+n));

%Second svd for U12'*U11*Sigma11
Second= U12'*U11*Sigma11;
[UNsing,SNsing,VNsing]=svd(Second);

%Calculation of Un
Un=UNsing(1:(2*p*r-n),1:n);

%Calculation of statespacevector
X2=Un'*U12'*Z1;

%Overdetermined equationsystem
Xk1=X2(:,2:s);
Xk=X2(:,1:s-1);
y=Y(:,r+1:s+r-1);
u=U(:,r+1:s+r-1);
xk1y=[Xk1;y];
xku=[Xk;u];
ABCD=xk1y*pinv(xku);
A=ABCD(1:n,1:n);
B=ABCD(1:n,(n+1):(n+m));
C=ABCD((n+1):(n+p),1:n);
D=ABCD((n+1):(n+p),(n+1):(n+m));

%Residuals
W=Xk1-A*Xk-B*u;
E=y-C*Xk-D*u;
```

hankel.m

```
[YH,UH]=hankel1(Y,U,p,m,N,r,timeshift);
%This function creates a Hankelmatrix with
%timeshift
%and returns UH and YH
%Jonas Ekblad 951101
%r - number columns of timevaluevectors in
%Hankelmatrix
%N - number rows of timevaluevectors in
%Hankelmatrix

for j=0:(r-1)
 for i=1:N
  YH((j*p+1):(j*p+p),i)=Y(1:p,(i+j+timeshift));
  UH((j*m+1):(j*m+m),i)=U(1:m,(i+j+timeshift));
 end;
end;
```

coord.m

```
function [K]=coord(U)
%Computes coordinates xyz, x lateral, y up-down, z
sagittal
%U - inputmatrix with voltages X1,Y1,X2 and Y2
%gamma1 - horisontal angle between Cam1's
zeroline and LED
%gamma2 - '    "      "    Cam2's   "      "
%alfa - angle between the two cams lines of zero
%D - distance between zeropoint and cam plane
%Dist1,Dist2 - distance camera-lens LED's
projection on zeroline
%R1,R2 - distance camera point of convergence
%X1,Y1,Z1 - coordinates with cam1 as referens
%X2,Y2,Z2 -    "          cam2      "
%X,Y,Z - real coordinates
%Jonas Ekblad 951015

D=63;
alfa=2*pi/15;
R=D/(2*sin(alfa/2));

%Computation gamma
 gamma1=(atan (0.0401*U(:,1)));
 gamma2=(atan (0.0405*U(:,3)));

%Computation of X1 Y1 Z1
 Dist1=D*(sin(pi/2-alfa/2-
gamma2)).*cos(gamma1)./(sin(alfa-
gamma1+gamma2));
 X1=U(:,1).*(0.0401*Dist1+0.3399);
 Y1=U(:,2).*(0.0399*Dist1+0.5614);
 Z1=R-Dist1;
 K1=[X1,Y1,Z1];

%Computation of X2 Y2 Z2
 Dist2=D*(sin(pi/2-
alfa/2+gamma1)).*cos(gamma2)./(sin(alfa-
gamma1+gamma2));
 X2=U(:,3).*(0.0405*Dist2+0.2637);
 Y2=U(:,4).*(0.0423*Dist2+0.2086);
 Z2=R-Dist2;
 K2=[X2,Y2,Z2];


%Computation of real coord-CAM1
 X11=X1*cos(alfa/2)+Z1*sin(alfa/2);
 Z11=-X1*sin(alfa/2)+Z1*cos(alfa/2);
 K11=[X11,Y1,Z11];

%Computation of real coord-CAM2
 X22=X2*cos(alfa/2)-Z2*sin(alfa/2);
 Z22=X2*sin(alfa/2)+Z2*cos(alfa/2);
 K22=[X22,Y2,Z22];

%Real coord
 X=0.5*(X11+X22);
 Y=0.5*(Y1+Y2);
 Z=0.5*(Z11+Z22);
 K=[X,Y,Z];
 end;
```